

Why meteors rock

An analysis of radio meteor detection

Charles Powell

March 24, 2017

Abstract

In this report I present 6 chapters, each a distinct study on meteor detection rates from observers across the world. Firstly, I analyse the phenomenon of diurnal shift, presenting a model linking Earth's orbital velocity and daily increases in rates. Secondly, through analysis of spatial and antenna type variation, I find that radio methods yield similar results to visual detection, as expected. There is little variation in the characteristics of meteor detection rates globally, nor between antenna types. Following from this, my analyses of temporal variation show evidence of a link between detection rate maxima and solar cycle minima, as found by other studies. Penultimately, I develop an improved correction of shower radiant height, which when applied to zenithal hourly rate (ZHR) calculations, demonstrates the validity of application to radio meteor detection, producing results reflecting those of visual observation. However, further refinement of population index models are necessary. Finally, I investigate methods of image analysis, focused on root mean square difference, finding a good correlation with other radio detection results, giving an adaptable new method.

Contents

1	Introduction	4
1.1	Motivations	4
1.2	Background	4
1.2.1	What is a meteor?	4
1.2.2	Radio meteor detection	4
1.2.3	Meteor showers	5
1.2.4	Magnitude	5
2	Data	7
2.1	Where is the data from?	7
2.2	What is the data?	7
2.3	Data collection & storage	8
2.4	Final data set	8
3	Diurnal Shift	10
3.1	Background	10
3.2	Literature Review	10
3.2.1	Model	10
3.2.2	Previous analyses	10
3.3	Methodology	11
3.3.1	Spatial analysis	11
3.3.2	Temporal analysis	11
3.4	Results & Discussion	11
3.4.1	Model	11
3.4.2	Sine function fit	12
3.4.3	Spatial variation	13
3.4.4	Temporal variation	15
3.4.5	Improvements	16
3.5	Conclusion	16
4	Spatial variation of data characteristics	17
4.1	Background	17
4.2	Literature Review	17
4.3	Methodology	17
4.4	Results	18
4.4.1	Latitude analysis	18
4.4.2	Longitude analysis	19
4.5	Discussion	22

4.5.1	Latitude analysis	22
4.5.2	Longitude analysis	22
4.5.3	Improvements	23
4.6	Conclusion	23
5	Temporal Variation of Radar Counts & Data Characteristics	24
5.1	Overview	24
5.2	Literature Review	24
5.3	Methodology	25
5.3.1	Data characteristics	25
5.3.2	Detection counts	25
5.3.3	Analysis by location	25
5.4	Results	25
5.4.1	Data characteristics	25
5.4.2	Monthly scale variation	26
5.4.3	Annual scale variation	27
5.4.4	Variation since 2000	27
5.5	Discussion	28
5.5.1	Data characteristics	28
5.5.2	Monthly scale variation	28
5.5.3	Annual scale variation	28
5.5.4	Variation since 2000	28
5.6	Conclusion	29
6	Antenna Data Characteristics	31
6.1	Background	31
6.2	Methodology	31
6.2.1	Selecting authors	31
6.2.2	Analyses	31
6.2.3	Sample sizes	32
6.3	Results	32
6.3.1	Mean & maximum	32
6.3.2	Standard error	32
6.3.3	Skew	32
6.3.4	Diurnal shift	33
6.4	Discussion	34
6.4.1	Mean & maximum	34
6.4.2	Standard error	34
6.4.3	Skew	34
6.4.4	Diurnal shift	34
6.4.5	Improvements	34
6.5	Conclusion	35
7	Zenithal Hourly Rate Validity for Radio Detection	36
7.1	Background	36
7.2	Literature Review	36
7.2.1	Calculating ZHR	36
7.2.2	Meteor shower information	37
7.3	Methodology	37
7.3.1	Assumptions	37

7.3.2	Formula modification	37
7.3.3	Calculating radiant height	39
7.3.4	Calculating hourly rate	39
7.3.5	Analysis	39
7.4	Results	40
7.4.1	Comparison	40
7.4.2	Correction factors	42
7.5	Discussion	43
7.5.1	Comparison	43
7.5.2	Correction factors	44
7.5.3	Formula improvements	44
7.5.4	Inaccuracies	45
7.6	Conclusion	45
8	Meteor Detection by Root Mean Square Difference Image Analysis	46
8.1	Overview	46
8.2	Methodology	47
8.2.1	Root mean square difference	47
8.3	Results	48
8.3.1	Data	48
8.3.2	Correlation	48
8.4	Discussion	49
8.4.1	RMS difference	49
8.4.2	Alternative methods	49
8.5	Conclusion	50
9	Conclusion	51
9.1	Comments	51
9.2	Main findings	51
9.2.1	Diurnal shift	51
9.2.2	Spacial variation of data characteristics	51
9.2.3	Temporal variation of radar counts & data characteristics	51
9.2.4	Antenna data characteristics	51
9.2.5	Zenithal Hourly Rate (ZHR) validity	52
9.2.6	Meteor detection by RMS difference image analysis	52
9.3	Acknowledgements	52
Appendices		53
A	Zenithal hourly rate results	54

Chapter 1

Introduction

1.1 Motivations

To all but the dinosaurs, meteors are quite cool. I must first admit that I have lied to you: this report is not about why meteors rock. In fact, half of meteors *aren't* made of rock, but it got your attention, didn't it? And now you're reading this! In this report I provide an analysis of a variety of variables that apply to meteor detection. Each of these analyses has its own significance purely to be known, though I have decided to venture into this EMC project out of my own interest in the subject. Much of the work in this report has been an intention of mine for a year or two, as a product of working with colleagues in the Lockyer Technology Centre (LTC) at the Norman Lockyer Observatory (NLO).

1.2 Background

1.2.1 What is a meteor?

Meteoroids are rocky or metallic bodies much smaller than asteroids, which, despite sizes ranging from a grain of sand to centimetres wide, produce streaks of light from the intense heat vaporising the meteoroid. At this point, it is a meteor. It is a matter of debate whether the meteor is the object causing the streak across the sky, or the streak itself. Meteors that survive the plummet to Earth are promoted to meteorites.

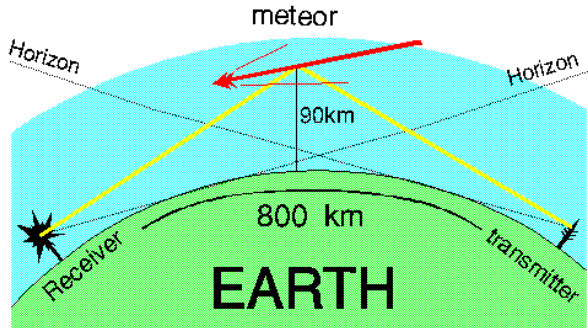


Figure 1.1: Diagram of forward scatter radio meteor detection (courtesy of [22])

1.2.2 Radio meteor detection

The intense heat of a meteor ionises the air around it, causing the visible streak seen in the sky. The ionised air along the path of the meteor is capable of reflecting radio waves, allowing a signal to be received. This is radio meteor detection. The diagram for detection is shown in figure 1.1. The transmitting antenna sends out a signal that reflects off of the ionised trail and is received by another station. The data that comes from detecting these ionised trails can be visualised in various ways; most popularly by simply counting the number of detections an hour, or more visibly by displaying the intensity of the reflected signal for a range of frequencies against time. This produces a rather beautiful ‘waterfall’ plot, seen in figure 1.2. The ‘echo’ received from the meteor has a characteristic shape depending on whether upper sideband (USB) or lower sideband (LSB) is used. In figure 1.2a, USB is used, producing an echo that trails off to the right, and has a peak to the left.

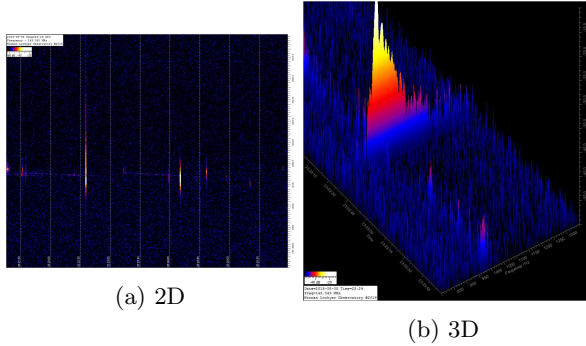


Figure 1.2: Waterfall plot

The colour of the peak indicates the intensity of the received echo. The blue noise surrounding the echo is radio noise.

The alternative method, counting the number of meteors detected in an hour, is discussed in chapter 2.

1.2.3 Meteor showers

Typically, visual observation of meteors is done during a meteor shower. This event is characterised by an increased number of meteors observed, that are not sporadic. Sporadic meteors are those that do not appear to come from a common source — they are simply debris entering the Earth’s atmosphere. During a meteor shower, many more meteors are observed than normal, and most importantly, they appear to come from a common source: the radiant. This is the *apparent* source of all the shower meteors: the meteors appear to travel out in all directions from this point.

The cause of a meteor shower is the Earth passing through the trail of debris left by a comet: dirty snowballs (figure 1.3). The only (notable) exception to this is the Geminids shower, which is caused by a Palladian asteroid rather than a comet’s trail [6]. The debris can be produced in many different ways, either through water vapour drag [2], in which ice melts and drags sand and pebble sized debris off the comet, or the breakup of parts of a comet.

As time passes, the stream will pass around the Sun and spread out. This means that, with time, a meteor shower’s peak will become less pronounced

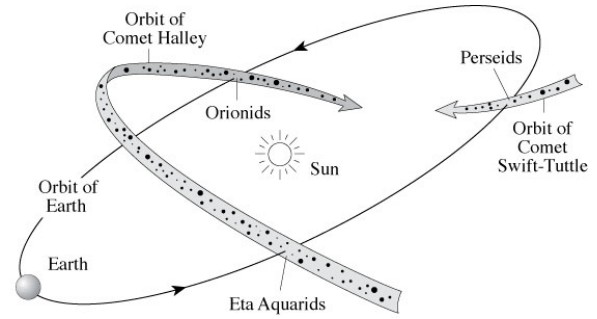


Figure 1.3: Meteor stream diagram (courtesy of [12])

as the meteoroids spread out across the entire orbit of the debris. However, showers caused by periodic comets will not suffer this effect since with each of the comet’s orbits, more debris is shed.

The most famous meteor showers include the Perseids, which often have the greatest number of meteors observed, and peak on the 12th or 13th of August. The Leonids originally gave birth to the name ‘meteor shower’, after a meteor ‘storm’ in 1833 producing thousands of meteors a minute (figure 1.4). This occurs once every 33 years (on average). Other showers, such as the Taurids, do not produce as many meteors, but are notable for frequent fireballs. These are meteors that explode due to the incredible pressure and heat of re-entry, and cause a sudden flash of light that can often illuminate the whole sky.

1.2.4 Magnitude

A measure of brightness used within Astronomy is magnitude. The magnitude scale is logarithmic and historically based around a single star, α Lyrae, which was used as the 0 point, though it is now defined in terms of flux. A decrease in magnitude by 1 means a brightness increase of $\sqrt[5]{100} \approx 2.512$. The larger the magnitude of a star, the fainter it is. Negative magnitudes are possible: for example, the Sun has an apparent magnitude of -27 . Apparent magnitudes are a measure of brightness from Earth, whilst absolute magnitudes are an objective measure of brightness, being the theoretical brightness of a star from a set distance (1 parsec). For visual observation (naked eye), meteors fainter

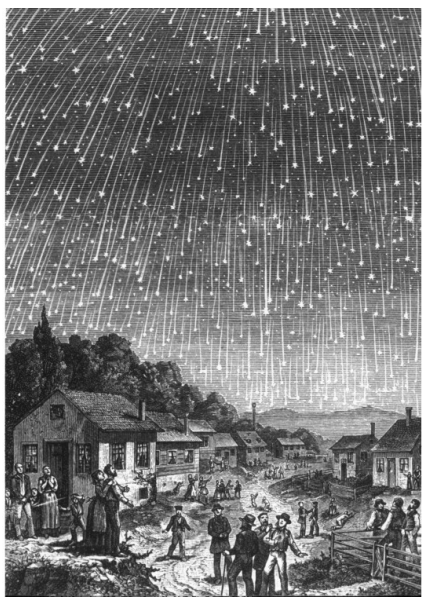


Figure 1.4: Leonids shower November 1833 (courtesy of [17])

than 6.5 in apparent magnitude cannot be seen. This is not the case for radio meteor detection.

Chapter 2

Data

2.1 Where is the data from?

The Radio Meteor Observing Bulletin (RMOB) [21] is an organisation of people from the field of radio meteor scatter observations and data reduction. Started in August 1993, the intention was to enable easy communication of data from the Perseid meteor shower. In the years that followed the bulletin became monthly and now has hundreds of observers in various locations around the world. The long-term aim is to cover the *entire* world, allowing detection of stream outbursts that will not be noticed visually.

Pierre Terrier, an RMOB member, has developed software that allows observers to upload data to a database on the RMOB website (rmob.org [21]). This is the source of my data, providing a range of data dating back to 2000 from observers across the globe.

2.2 What is the data?

The data provided by RMOB is a text and image collection, as in figure 2.1.

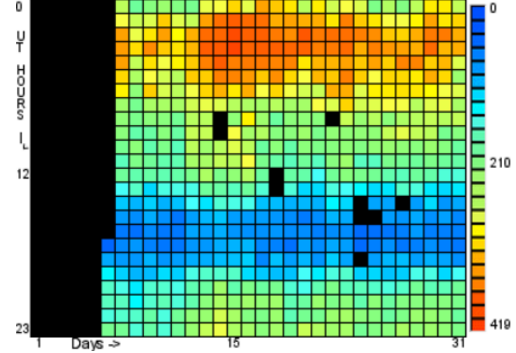
The data is collected using the observer's own radio setup. This will include an antenna, and a way of getting the signal to the computer. Typically this is done using a receiver (to control properties of the signal such as squelch) which feeds into the audio port of a computer or laptop. The software works in two parts.

The first stage is detecting the meteors from the signal. This is done using HROFFT [18] (figure 2.2).

As can be seen in figure 2.2, the intensity of the signal is calculated and shown in a light blue colour. The full waterfall plot is shown above this, making

jan 00h 01h 02h 03h 04h 05h 06h 07h 08h 09h 10h 11h 12h 13h 14h 15h 16h 17h 18h 19h 20h 21h 22h 23h
01 123 124 125 126 127 128 129 130 131 132 133 134 135 136 137 138 139 140 141 142 143 144 145 146 147
02 177
03 177
04 177
05 177
06 177
07 177
08 177
09 177
10 177
11 177
12 177
13 177
14 177
15 177
16 177
17 177
18 177
19 177
20 177
21 177
22 177
23 177
24 177
25 177
26 177
27 177
28 177
29 177
30 177
31 177

(a) Text format



(b) Image format

Figure 2.1: RMOB data formats

up the main part of the screen, much the same as figure 2.1b. When the intensity of the signal goes over a threshold, it is noted as a meteor (yellow spike). The first threshold is 25dB, the second is 50dB and the third is 75dB. This information is then passed onto Colorgramme Lab. In Colorgramme Lab, the counts are converted to text format and stored as seen in figure 2.1a. At the end of the month, this data is uploaded to RMOB.

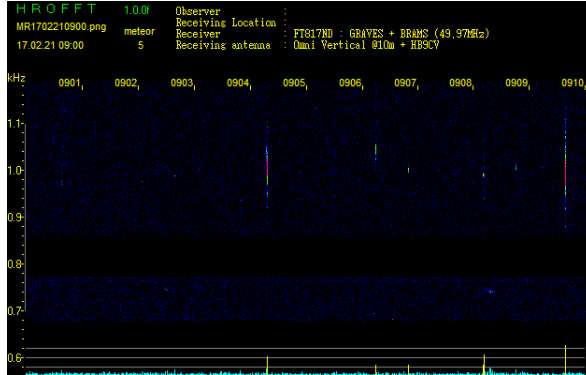


Figure 2.2: HROFFT software screen (courtesy of [16])

2.3 Data collection & storage

Collection

I have collected the data using web scraping. This is a process where a program (mine is written in Python) goes to a webpage, finds all the links on the page, and returns them. By going through each page of data available on the website, I could then download each text file, for each observer, for each month, for each year.

Storage

I created two ‘objects’ in Python in order to store the data. Objects are similar to real life objects — self-contained elements that have their own properties. In the case of the RMOB data, it can be easily split into observers (the stations or people detecting the meteors) and ‘entries’: monthly collections of data (a single text file from RMOB).

Using the links collected from web scraping, each file was downloaded, formatted, and loaded into an entry. The data is not stored as part of the entry: the formatted file is saved to a folder. The formatting itself is so that the data is easy to use. Instead of storing the counts using “|” to separate the hours, I am using simple commas (“,”) to separate the hours. Instead of using “???” to denote unavailable data, I am using “-1”. This makes it easier both to load the data, and to remove empty data.

Each entry has properties: the source of the data (the location in my filesystem that the data is

stored), the date (in the format YYYY-MM) and the data itself. Storing every single item of data would be inefficient, so the data must be loaded by calling `entry.loadData()` first. This opens the location in my filesystem, loads the .csv file, and thus makes the data available for processing.

Each of these entries is stored in an ‘observer’ object. This is done by storing the entries in a dictionary, so that the correct data can be selected by specifying the month which is associated with the month of the entry. Some RMOB text files include properties of the detection setup, such as antenna, location, and frequencies. These are stored as part of the observer object as attributes. This allows an easier analysis, since while (for example) assessing spatial variation, the GMAP location can be selected by typing `observer.locationAttr['latitudeGMAP']`. Where two entries for the same observer differ, there is a ‘collision’. In this event, two separate observers are stored.

2.4 Final data set

Figure 2.3 shows how many observers contributed to RMOB each month since 2000. Overall, there are 345 observers in my data set, with 5110 entries in total. This means, at most, I have 3,800,000 hourly counts. As can be seen in the figure, more and more observers are uploading each month. This can only mean good things for radio meteor detection analysis!

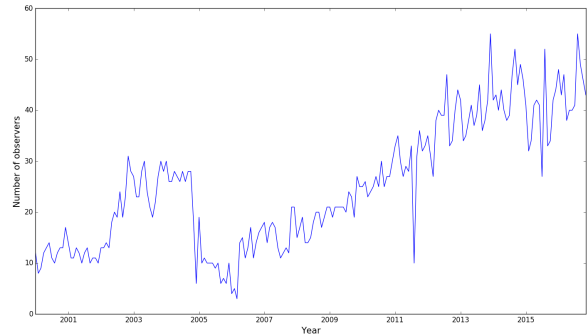


Figure 2.3: Number of observers contributing each month

Figure 2.4 shows the locations represented in the data set. There is clearly a wide variety of loca-

tions, across the globe, which will make an analysis of spatial variation valid and worthwhile.

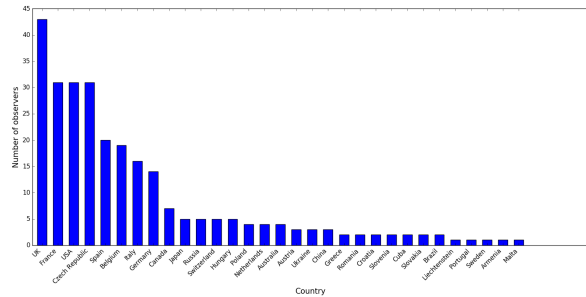


Figure 2.4: Locations of observers (where known)

Figures 2.5 and 2.6 show the volume of data available for each country, and the average number of entries uploaded each month.

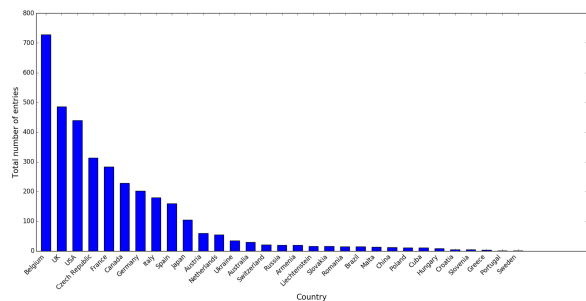


Figure 2.5: Volume of data from each location (where known)

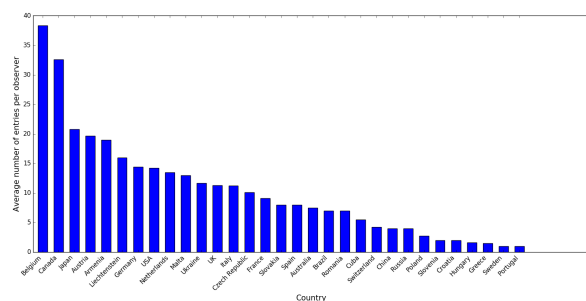


Figure 2.6: Average number of entries per month from each location (where known)

Chapter 3

Diurnal Shift

Abstract

I present an improved model of diurnal shift, aiming to resolve issues evident in previous models and be more mathematically rigorous. I investigate the apparent sine-function variability of hourly meteor counts, as well as the temporal and spatial variation of said counts. My findings indicate that diurnal shift is dependent on Earth's orbital velocity, producing a clear trend between longitude and peak hour. I find no evidence of correlation between latitude and amplitude of diurnal variation.

3.1 Background

For years, a notable increase and decrease over a single days' time scale has been observed in detection counts. An example of this is in figure 2.1b. The red colours indicate a higher detection count, observed in the early hours of the morning. This diurnal shift *has* been given an explanation by modelling the phenomenon. The word 'diurnal' refers to the time scale being a single day, and 'shift' refers to the increase in detection counts.

3.2 Literature Review

3.2.1 Model

Dr David Morgan of the BAA Radio Astronomy Group presents a somewhat detailed explanation [13] of why diurnal shift occurs. The suggestion is that diurnal shift is dependent on sporadic meteors rather than shower meteors, and depends on the variation of their intercept velocity with an observer on Earth. This changes because as the Earth rotates, the combination of the orbital velocity, rotational velocity and meteor intercept velocity changes. As can be seen in figure 3.1 (courtesy

of the same article [13]), at sunrise, the meteor's velocity *adds* to Earth's orbital velocity, whilst at sunset, these velocities *subtract*.

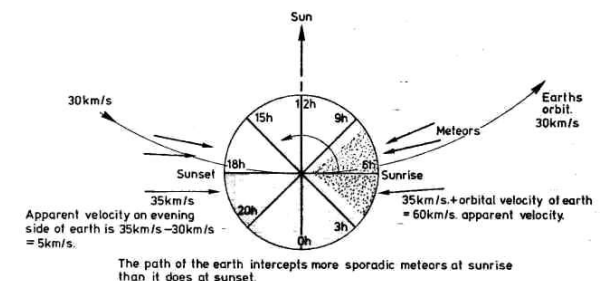


Figure 3.1: Diurnal shift model

3.2.2 Previous analyses

Diurnal variation is well studied. Singer, W., von Zahn, U. and Weiß, J. present an analysis [8] of the diurnal and annual variations of meteor rates at the Arctic circle, specifically the ALOMAR observatory. They observe a clear diurnal shift, as well as an annual variation of this diurnal shift. The expectation that the intensity of the diurnal shift decreases towards the North Pole is not observed.

Category	N° observers
Europe	220
Asia & Australia	12
North America	37

Table 3.1: Sample sizes for location categories

Singer, W., von Zahn, U., Batista, P. P., Fuller, B., & Latteck, R. present an analysis [10] of the same subject that *does* observe an increase in diurnal shift intensity with decreasing latitude, which disagrees with the previous article [8]. However, this analysis uses a wider range of latitudes to analyse, so the conclusion is likely more valid.

3.3 Methodology

In this analysis I will use previous results to examine spatial and temporal variation of diurnal shift, as well as how well a sine function fits the diurnal shift curve. The diurnal shift curve is generated by taking the mean of all data for a given hour after midnight, for each observer. Time, for all observers, is recorded in UTC. Using this curve I will compare the intensity of diurnal shift for three different location categories: Europe, Asia & Australia, and North America. The sample sizes for each category are shown in table 3.1. In conjunction with this, I will fit a sine curve, to give an indication of a suitable function to describe the shift.

3.3.1 Spatial analysis

I will use QGIS [20] to generate a map, with a dot representing each observer with a known location. These dots will be coloured based on the peak hour of diurnal shift, indicating how this changes with location. Further to this, I will analyse the variation of the peak hour of diurnal shift, as well as the sum of parameter standard deviation for a sine function of the form $A \sin\left(\frac{2\pi}{24}t + \phi\right) + \mu$, indicating how well a sine curve fits the diurnal shift. This is calculated using the reduced covariance matrix X and the reduced chi-squared χ^2 , where

$$\chi^2 = \frac{r^T Ir}{N - 3} \quad (3.1)$$

N is the number of data points, r is the matrix of residuals and I is the identity matrix. The numerator is the minimum value of the weighted objective function (the optimal parameters). Then, the variance-covariance matrix of the parameters M^β is;

$$M^\beta = \chi^2 (X^T X)^{-1} \quad (3.2)$$

The parameter standard deviations is $\sigma_i = \sqrt{M_{ii}^\beta}$, and the sum of these three is taken. This analysis will be over two independent variables: latitude and longitude.

3.3.2 Temporal analysis

Finally I will analyse how the peak hour and parameter standard deviations vary over time, from 2000 to 2016. This will use the same calculated variables as the spatial analysis. These analyses will be completed using a Python program.

3.4 Results & Discussion

3.4.1 Model

I aim to improve the model presented by Dr David Morgan [13].

Inaccuracies

The diagram and explanation have a few issues. Firstly, the diagram states (in conjunction with the explanation) that the path of the Earth intercepts more meteors at sunrise than sunset, causing the increase. This is not the case: the path of the Earth does not change, nor does the number of meteors being intercepted. What changes is the number of meteors that are intercepted that can be detected by a given observer. The explanation is suitable, but only if the cause is more rigorously explained as the velocity being proportional to the number of detections. When there is a greater velocity, more meteors can actually reach the Earth's atmosphere and be detected. This is where the explanation appears to fall down. The diagram shows meteors intercepting the Earth at sunset, and sunrise, but nothing in between. Perhaps this is an ambiguity, but the implication is that there is a sudden increase and decrease. As

is clear from the results, this isn't the case. The increase fits a sine curve remarkably well and the change occurs throughout the day. This suggests that the change, whilst it is indeed dependent on meteor intercepts, is a function applied to meteor velocities that is based on the angle of Earth's rotation.

Own Solution

Building upon the previous model, I assume that the number of meteors detected is proportional to the mean incident velocity of meteors to Earth. This is reasonable: the *actual* velocities are of course random. However, an overall larger mean incident velocity of a collection of meteors means that proportionally more will reach Earth, of those that are in a direction that *could* cause a collision with Earth's atmosphere. Of a group of meteors with random velocities (both random magnitude *and* direction), very few will be on a course tangential to Earth's atmosphere. However, this does not change as Earth rotates, so it is a negligible variable. I consider only those that are tangential with the atmosphere, and so only those that could cause a detection. Thus, we have, at a very basic level:

$$N \propto v_{\text{incident}} \quad (3.3)$$

The incident velocity is dependent on factors such as the Earth's rotational velocity, orbital velocity and the velocity of the sporadic meteors themselves. v_{meteor} is difficult to consider, since it (theoretically) has a random direction.

We know that $v_{\text{orbit}} \approx 30000 \text{ ms}^{-1}$ and $v_{\text{rotation}} \approx 450 \text{ ms}^{-1}$. Assuming that the path described by Earth's orbit around the Sun is a straight line through Earth when 'up close', let θ be the angle between a radius from the Earth's centre to the observer's location, and the orbital path (figure 3.2). The set of meteors that can be detected appear, from above, to form a triangle. The average velocity of these meteors will be along the height of this triangle: perpendicular to the surface of Earth (v_{meteor}). This means that the rotational velocity can be disregarded. Thus, the remaining velocity to consider is Earth's orbital velocity:

$$v_{\text{incident}} = v_{\text{orbit}} \cos \theta + v_{\text{meteor}} \quad (3.4)$$

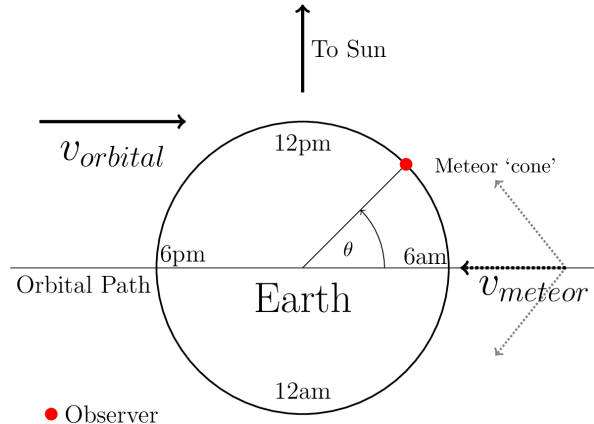


Figure 3.2: Diagram of model, showing an observer (red dot), the perceived meteor 'cone', and the incident meteor velocity v_{meteor} .

Clearly, this is at a maximum when $\theta = 0^\circ$. For an observer at a longitude of 0° , this is 6:00¹. Since this is where the angle is defined from, it is clear that for any observer the peak hour will be 6:00 local time (assuming local time is based off of longitude, not timezones). It should be noted that the peak hour can vary around this time, based on conditions for observing. Particularly important are changes in the ionosphere as the Sun rises, which stop reflection of radio signals, preventing erroneous detections and allowing for better reception of signals solely from transmitting antennas, providing better conditions for radio meteor detection. This could slightly shift the peak hour to be later than 6:00.

3.4.2 Sine function fit

Figure 3.3 shows the results for a sine function fit. The optimal sine function and cubic are shown in red and green respectively. The sum of the standard deviation for each parameter of the optimal sine curve (of the form $A \sin(\omega t + \phi) + \mu$) is 0.814, which indicates a positive correlation. This suggests (as is clearly apparent from the figure) that the sine function fits well. As a reference, I fitted a cubic. This shows how well a sine curve fits in comparison. The implication of this is that the cause

¹All times are in 24-hour format.

of diurnal shift is based on a sine function of the Earth's rotation (i.e. the hour of the day).

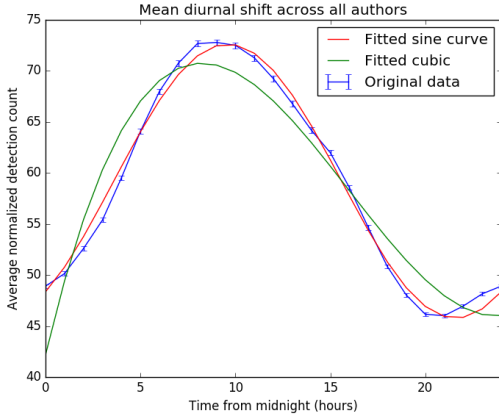


Figure 3.3: Diurnal shift across all authors & sine function fit

Figure 3.4 shows the same graph as figure 3.3 (for comparison), as well as diurnal shift curves for each respective location. Surprisingly, each location category shows a clear sine curve. The peak of these sine curves appears to be correlated well with latitude. The average longitudes in degrees are, for Europe, Asia & Australia, and North America respectively: $\sim 15^\circ$, $\sim 150^\circ$ & $\sim -100^\circ$. This supports the idea of a sine function describing the diurnal shift, since larger longitudes produce a greater hour of diurnal shift, bearing in mind that the hour for the North American category will ‘wrap’ around, due to timezones. The average latitudes in degrees are (respectively): $\sim 45^\circ$, $\sim 35^\circ$ & $\sim 15^\circ$. The North American category has the largest intensity, followed by the European category and then Asia & Australia, though this is not the order of latitudes. This appears to disagree with research noted in section 3.2.2, which suggested that the intensity (amplitude) of diurnal shift is dependent on latitude.

The sum of parameter standard deviations for each location category are shown below. The positive numbers all indicate a positive correlation, as expected from the figures.

3.4.3 Spatial variation

Created using QGIS, I present a map showing the location of each observer in the data set. The dot

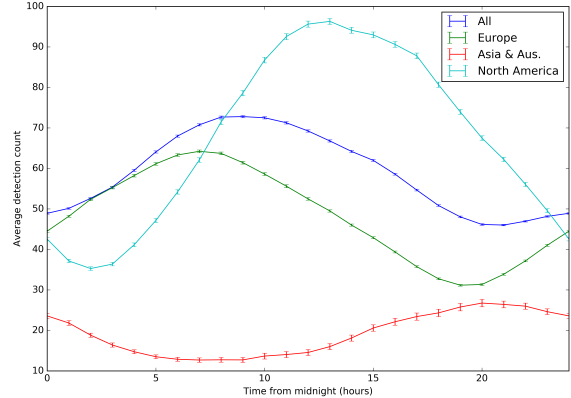


Figure 3.4: Diurnal shifts for each individual location (overall shift of all observers included for reference)

Category	A	ϕ	μ	$\Sigma\sigma$
All	13.4	-0.941	59.2	0.454
Europe	15.4	-0.302	48.4	0.498
Asia & Aus.	-7.19	-0.585	19.0	0.352
N. America	29.5	-2.05	68.1	1.16

Table 3.2: Sum of parameter standard deviations for each location category

for each circle is coloured (as in the legend) based on the peak hour of the diurnal shift. This gives a more visual demonstration of what is shown in figures 3.4 and 3.8: the colours are clearly grouped based on location. Observers in Europe have diurnal shift peaks mostly around 6:00, North American observers have peaks around 15:00 and in Asia & Australia around 20. This supports implications from the previously stated figures. There are clearly anomalous results for some observers (note the blue dots in Europe), though there is often anomalous data, so this is not unexpected.

Latitude

There appears to be little correlation between latitude and the peak hour. Although, overall, the hour appears to decrease as the latitude varies from -40° to 60° , their errors are substantial. The implication of this is there is little agreement within each category, suggesting no correlation at all. However, this is expected. There is no logical reason why the peak hour would be influenced by the latitude. Di-

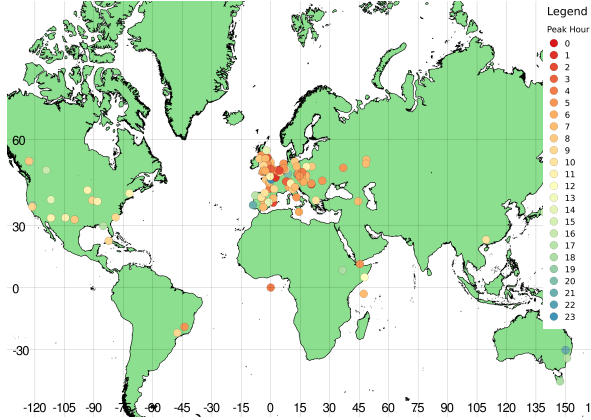


Figure 3.5: Peak hour of diurnal shift for each observer

urnal shift is caused (according to my model and [13]) by the Earth’s rotation changing the average incident velocity of meteors. This does not change with latitude, hence no correlation is seen.

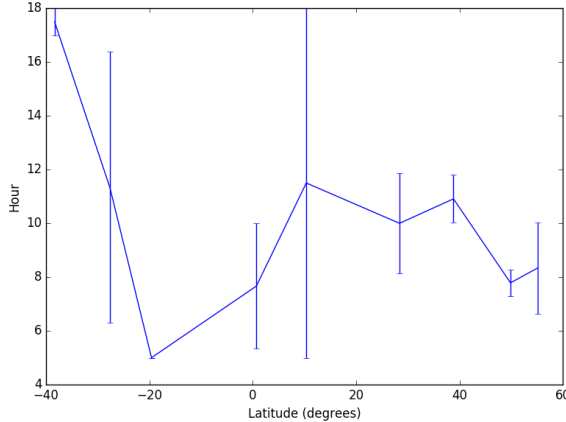


Figure 3.6: Peak hour of diurnal shift against latitude

In figure 3.7 little correlation is seen again. The standard deviations vary widely. There is no clear trend, suggesting that the latitude of an observer has no effect on how well data fits a sine function. Consequently, it would appear that diurnal shift is a global phenomenon.

Longitude

Figure 3.8 shows agreement with figures 3.4 and

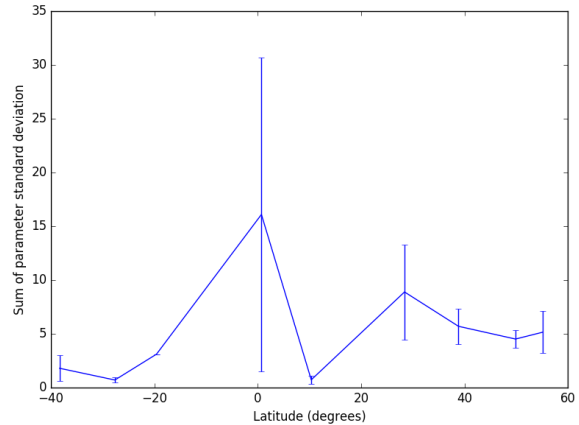


Figure 3.7: Optimal sine function fit against latitude

3.5. The peak hour is lowest for a longitude of 0° and increases either side of this, as seen in the stated figures. The errors for some categories are reasonably large, though still fall in a range that fits the trend. There is, of course, minor variation though the trend is clear from the data: latitude and peak hour of diurnal shift are related.

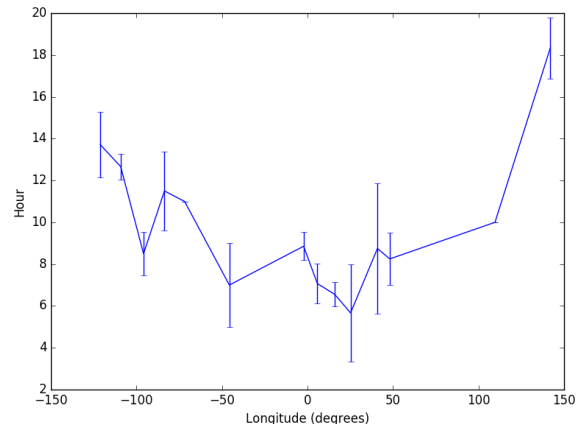


Figure 3.8: Peak hour of diurnal shift against longitude

In order to investigate this apparent trend further, I corrected the peak hour of each location category such that $H_{\text{corrected}} = H_{\text{calculated}} + \frac{\phi}{15}$, provided the longitude ϕ is in degrees. This means that the hour will be the local time (not using timezones, only the time based on longitude). This is shown

in figure 3.9. Errorbars, in this case, are such that 75% of the data for a given location category falls within the bars. The values appear to fluctuate around a peak hour of 6:00 (shown in green), supporting the model I have proposed. However, there is a large degree of variation.

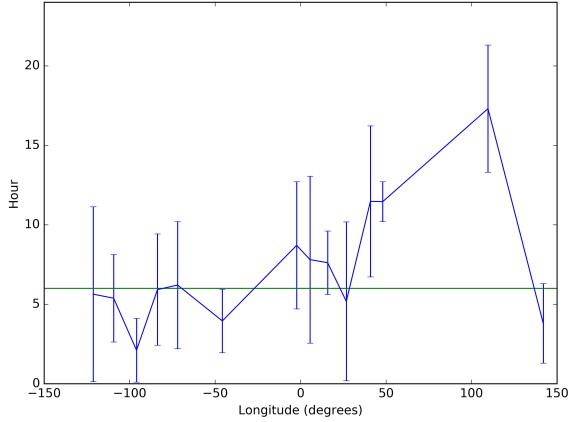


Figure 3.9: Corrected peak hour of diurnal shift against longitude

In figure 3.10 a histogram of the peak hour is shown. It is clear from this figure that the model is supported. Clearly most of the observers have a peak hour around 6:00, with some having a peak hour of 7. This is reasonable; as noted in section 3.4.1, the peak hour can in fact be slightly after 6:00, since changes in the ionosphere occur around this time, as the Sun comes over the horizon. This can improve radio detection, allowing for better conditions that would shift the peak hour. Of course, there is some distribution either side of 6:00, though this is expected.

The standard deviation varies a small amount with longitude. However, there are some categories with much larger variation. There does not appear to be a clear trend. However, the poorest fits have large errors indicating that this is not a poor fit throughout observers in said categories. Consequently it would seem that the fit varies moderately across the globe.

3.4.4 Temporal variation

Figure 3.12 shows the same result as previously noted. The variation for each location category

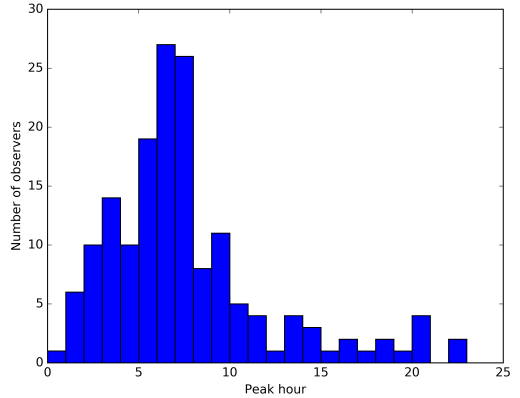


Figure 3.10: Histogram of peak hours

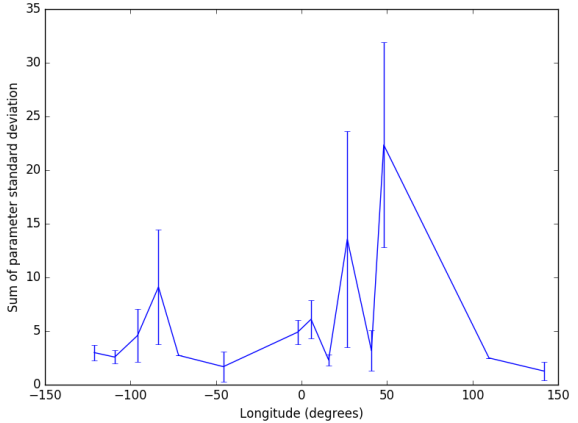


Figure 3.11: Optimal sine function fit against longitude

varies around the hours expected if peak hour is correlated with longitude. There is a large amount of variation for the Asia & Australia category, so it is hard to make an analysis from this. It is clear that in more recent years, there is less variation. Over time, no categories appear to increase or decrease, but instead fluctuate around certain values. Generally, the fit is reasonably good. Between 2005 and 2011, the fits are much worse, indicating either a weaker diurnal shift (an unlikely phenomenon) or a more intense background level. For periods outside this, there is a low value of variation. All categories have a similar fit and absent trend over time.

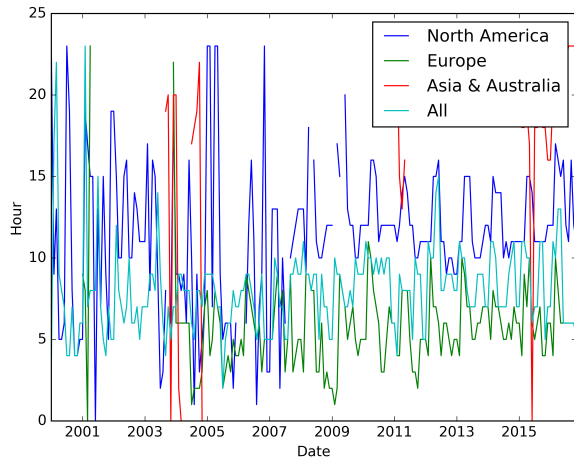


Figure 3.12: Peak hour of diurnal shift change over time

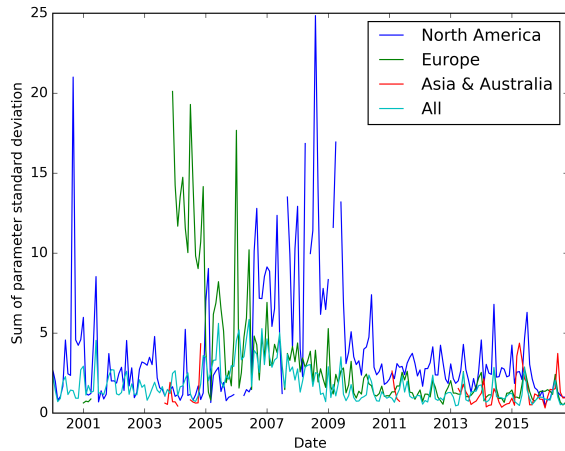


Figure 3.13: Optimal sine function fit change over time

3.4.5 Improvements

Annual variation

A question, that may reveal more information on the processes behind diurnal shift, is whether the phenomenon changes on a yearly time scale. Seasonal variation of diurnal shift may indicate an influence from sources such as the Sun, or the orientation of the Earth relative to its orbit.

Intensity variation with latitude

Singer, W., von Zahn, U., Batista, P. P., Fuller, B., & Latteck, R. [10] analyse a variation of diur-

nal shift amplitude with latitude. Their analysis is over a relatively small range of latitudes. A further investigation, with a wider range of latitudes and more observers involved, could confirm or support their analysis. My own analysis indicates that there is little correlation.

Receiving station vs. detection station

Most meteor detection setups are simply receiving stations. Typically a station, often a considerable distance away, emits a signal that reflects off of the meteor's ionised trail and is received by the observers, whose data are under consideration. This means that there is a difference between the longitude of the observer and the longitude of where the detection takes place. This will, of course, influence the conclusions made. Were the longitude of each detection station known, it may further support the conclusions of my model.

3.5 Conclusion

There is a clear correlation between longitude and peak hour of diurnal shift, as suggested by the model I propose. This is apparent from several results, including a histogram of peak hours. This good agreement indicates that my model is valid and is supported by the data. In addition, based on this analysis and previous analyses, it seems that there is little correlation between location and a sine function fit, suggesting that the intensity of diurnal shift (in the sense of relative intensity compared to background rates) is roughly uniform across the globe. However, there is no clear link to be made between the amplitude of diurnal shift and latitude. There appears to be a correlation, in general, with location, with a clear difference in amplitude between different location categories.

Chapter 4

Spatial variation of data characteristics

Abstract

In the following chapter I present an analysis of variation of data characteristics by latitude and longitude. I find little correlation between data characteristics and latitude, and a limited correlation with longitude. However, I find supporting results for a model of diurnal shift. A symmetric distribution for meteor counts is suggested from the results.

4.1 Background

The significance of this analysis includes a supporting argument for diurnal shift (see chapter 3), and potential identification of locations with particularly good detection counts, which has implications for the levels of radio noise where the detection takes place. An analysis of detection rates based on both longitude and latitude could yield results that beg an investigation: perhaps at higher latitudes there are more meteors travelling tangential to the atmosphere, giving more detections.

4.2 Literature Review

Unfortunately, no literature existed regarding this subject. Well, there is now!

4.3 Methodology

In this chapter I present two analyses on the variation of certain data characteristics by latitude and longitude. In order to carry out these analyses, the observers from the RMOB data must be split into

categories based on location.

Selecting observers

Observers were selected based simply on whether they had Google Maps (GMAP) co-ordinates available. These co-ordinates are entered when uploading data to RMOB and are stored as part of the observer class location attributes dictionary. Provided an observer had *both* latitude and longitude available, then the analysis would be carried out on this data. Once all the observers had been checked and analysed (if necessary), the categorisation into groups could take place. I used a basic process to group the observers, based on the difference between the current observer and the previous. The observers had to be sorted by increasing latitude or longitude (depending on the analysis) first. If the difference between co-ordinates was less than 10 degrees, then the two observers are considered part of the same group. This resulted in 9 categories for latitude, and 14 for longitude. These categories are not uniformly spread around the globe, but do provide a grouping of observers.

Analysis

These characteristics summarise the data,

namely 6 values: mean hourly count, max hourly count, skewness, peak hour of diurnal shift, fit to a sine function, and standard error. The standard error of all data for the observer is significant since it indicates how much the data varies over the time frame under consideration. A lower value indicates that the same detection count is generally seen, and a larger value indicates that the detection count varies erratically. The skew also indicates the distribution of the detection counts. A positive skew indicates that the detection counts trail off towards high values, whilst a negative skew indicates that the distribution is ‘steeper’ for higher values, suggesting that there is a limit to the detection counts. The last two values are the peak hour of the diurnal shift, and the fit to an optimised sine curve for the mean detection counts over each hour of a day. This is calculated by averaging the values for all data for a given hour after midnight. A sine curve is then fit to this, in the same process as chapter 3, giving a sine function of the form $N = A \sin(\omega t + \phi) + \mu$ where N is the detection count. The calculated ‘fit’ is the sum of the standard deviations for A , μ , and ϕ . ω is assumed to be $\frac{2\pi}{24}$ so that the shift has a period of one day. These 6 values will be calculated for each ‘entry’ (month) for each observer, and then a mean will be taken from all the results for a given location category.

4.4 Results

4.4.1 Latitude analysis

Sample sizes

Table 4.1 shows the sample sizes for each latitude category.

Category	Latitude range ($^{\circ}$)	Nº observers
I	-43 – -33	2
II	-31 – -22	3
III	-20 – -19	1
IV	-4 – 5	3
V	8 – 12	2
VI	23 – 33	5
VII	33 – 44	33
VIII	44 – 53	107
IX	54 – 57	9

Table 4.1: Sample sizes for latitude categories

Mean hourly detection count

As can be seen in figure 4.1, overall, the detection count is ~ 60 . There is a very low sample size for the category around a latitude of 0, which explains the large standard error. There does not appear to be an overall trend, there are no exceedingly anomalous results and there is no clear pattern across the categories. The minimum mean hourly detection count is category II ($\sim -30^{\circ}$) and the maximum is ($\sim 0^{\circ}$).

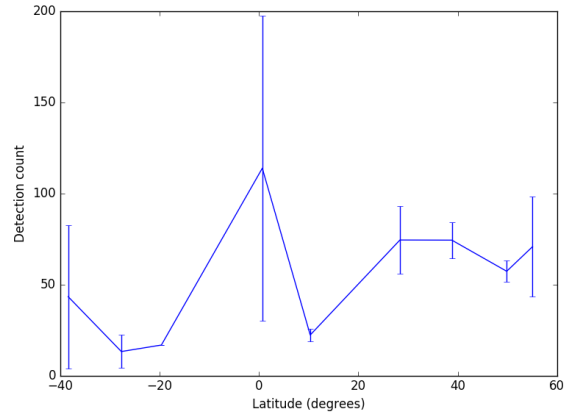


Figure 4.1: Mean hourly detection count

Maximum hourly detection count

The standard errors are generally larger for the same categories compared to the mean hourly count. This suggests there is a much larger variation in the maximum count within each category. There is no clear trend over the latitude categories, as there is a large peak in category IV as well as VII. The lowest maximum hourly count is category III.

Minimum hourly detection count

For categories I–VI the minimum is 1. This is as expected. Category IX has the largest minimum, though there is a large error, indicating the low sample size. Categories VII–IX are the only categories without a minimum of 0.

Skewness

Generally, the skewness is positive. There is a large error (relative to the values) indicating a widely varying skewness within each category.

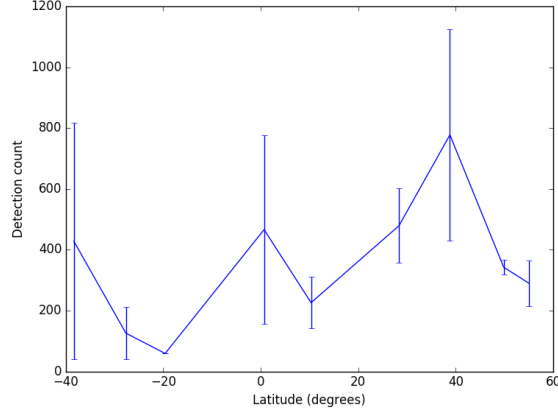


Figure 4.2: Maximum hourly detection count

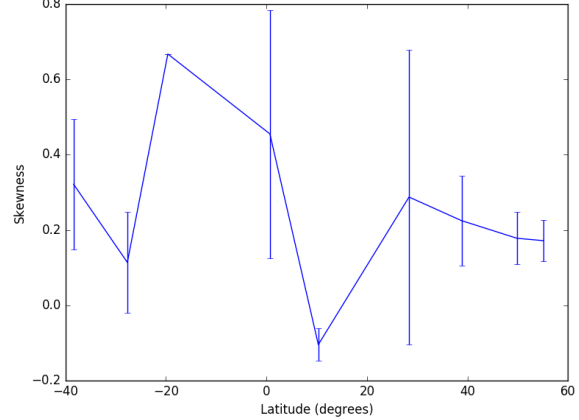


Figure 4.4: Skewness of hourly counts

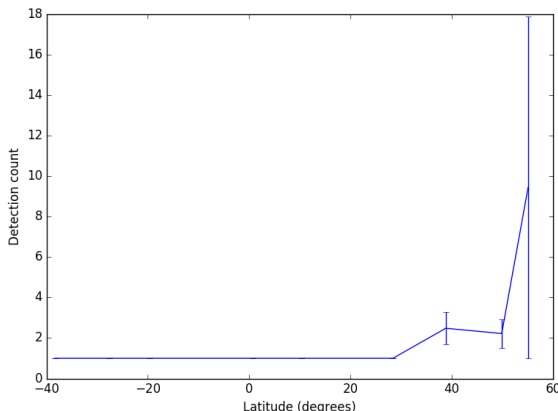


Figure 4.3: Minimum hourly detection count

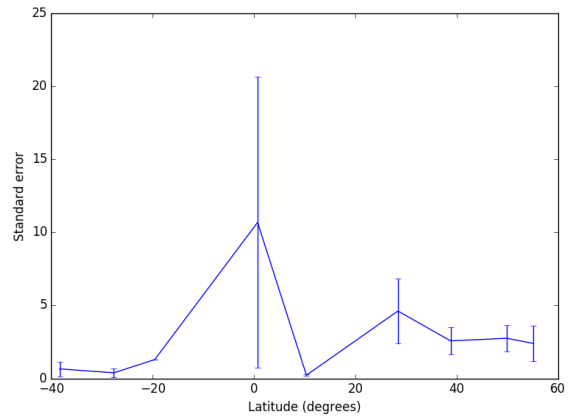


Figure 4.5: Variation in hourly detection count

There is no clear trend, though the skewness *appears* to decrease as the latitude increases. There is only one category (V) with a negative skewness.

Standard error

The standard error appears to be relatively low for most of the categories, and with similar values, varying only by ~ 3 . The only exception to this is category IV, which has the largest standard error of ~ 10 , though there is a much larger error in this than the other categories. This could simply be an anomalous reading.

Diurnal shift

There is no clear trend for the peak hour of the diurnal shift. There is a large error for most categories, for all categories having at least an error of 1 hour. The large error indicates a large amount of variation within each category.

For categories I–III and V, the fit is relatively good (~ 2). Categories VI–IX have a slightly worse fit, around 6. Rather anomalously, category IV has a very poor fit, though in figure 4.5 a large amount of variation is seen, so this is expected.

4.4.2 Longitude analysis

Sample sizes

Table 4.2 shows the sample sizes for each longi-

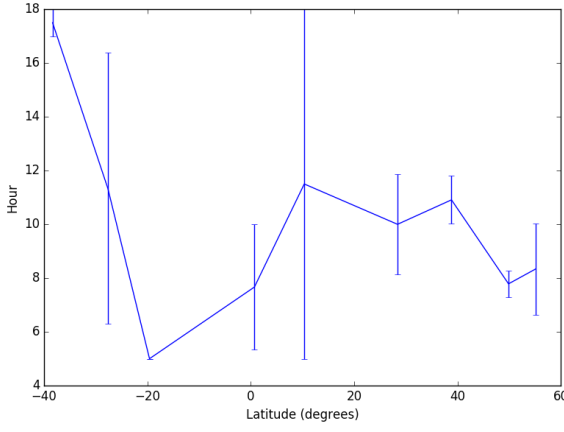


Figure 4.6: Peak hour of diurnal shift

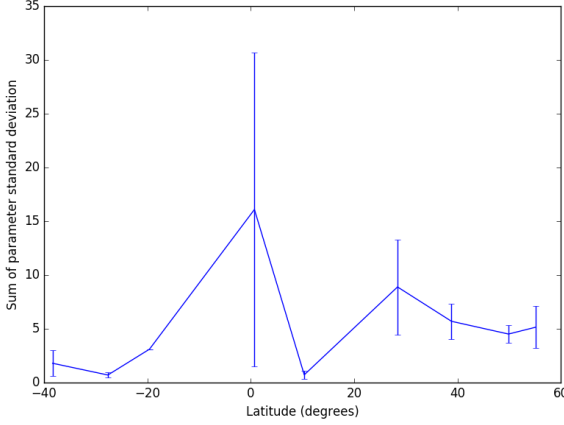


Figure 4.7: Fit of diurnal shift to an optimal sine function

tude category.

Mean hourly detection count

There is no clear trend for the mean hourly count. The lowest mean is ~ 10 , for category VI. The maximum is XII, with a mean hourly count of more than 200. The errors are smallest for the categories with the largest sample sizes, namely categories VII–IX.

Maximum hourly detection count

Most maximum hourly detection counts are around 500, though there is an anomalous maximum for category X, with a maximum of more than

Category	Longitude range ($^{\circ}$)	Nº observers
I	-123 – -114	7
II	-112 – -104	6
III	-100 – -90	4
IV	-88 – -78	4
V	-72 – -71	1
VI	-48 – -44	2
VII	-9 – 0	56
VIII	1 – 12	32
IX	12 – 21	34
X	22 – 32	5
XI	36 – 46	4
XII	47 – 49	4
XIII	109 – 110	1
XIV	139 – 148	3

Table 4.2: Sample sizes for longitude categories

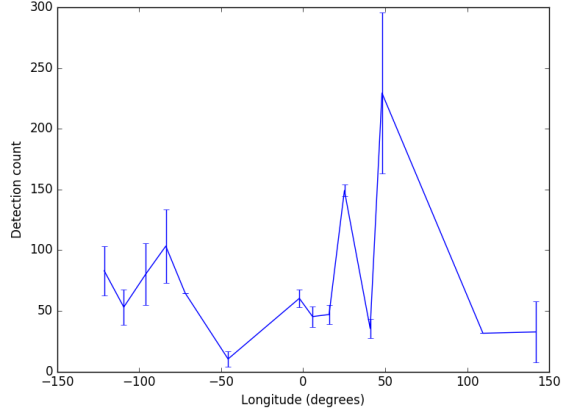


Figure 4.8: Mean hourly detection count

4000. This is likely only a single observer, however, as indicated by the low sample size and large error.

Minimum hourly detection count

The minimum values are, unlike in figure 4.3, not all 1. Most are a low value, though there is an anomalous result for XII, similar to the mean hourly count. This anomalous result is reflected by the large error.

Skewness

9 out of 14 categories are positive. This is similar to figure 4.4. There is a large error for most

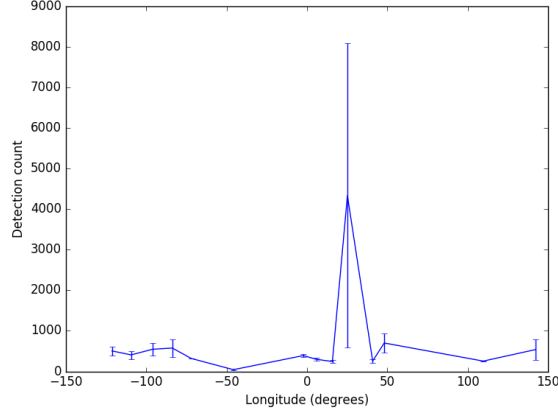


Figure 4.9: Maximum hourly detection count

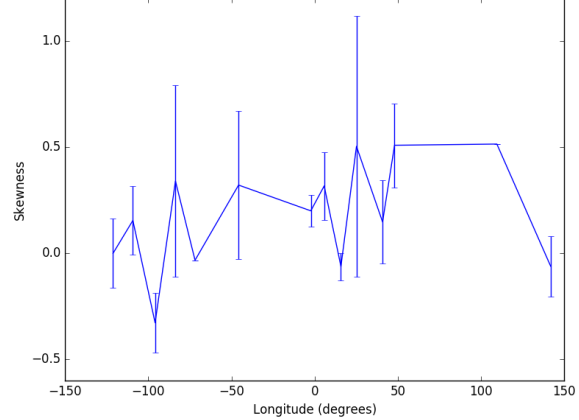


Figure 4.11: Skewness of hourly counts

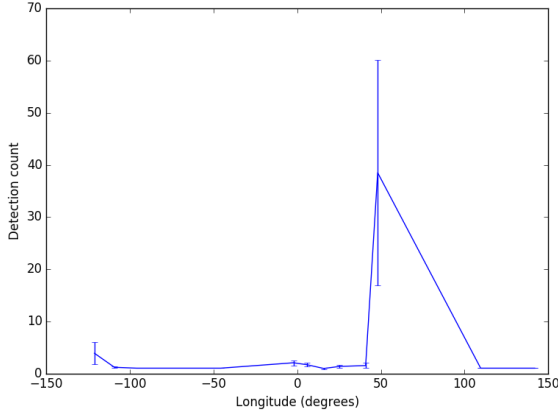


Figure 4.10: Minimum hourly detection count

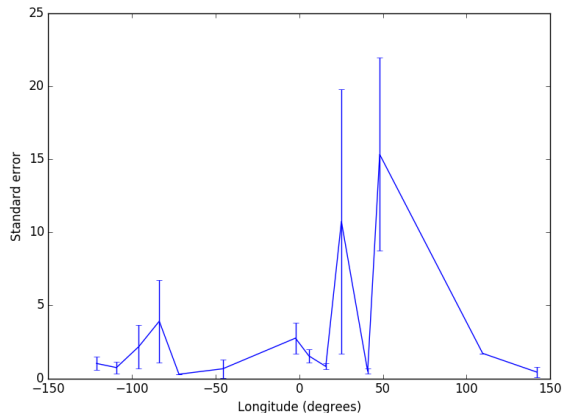


Figure 4.12: Variation in hourly detection count

categories, indicating a large amount of variation within each category. This suggests there is little correlation between longitude and skewness of hourly counts.

Standard error

Figure 4.12 shows that there is a relatively low variation for most categories. The exceptions are categories X and XII, with errors of ~ 10 and ~ 15 respectively. There is a small error for all other categories, indicating a similar level of variation within the category.

Diurnal shift

There appears to be a correlation between lon-

gitude and the peak hour of diurnal shift. This is discussed in more detail in chapter 3. The peak hour is lowest for low longitudes, around 6, and larger for large latitudes, approximately 14 for a longitude of -125° and 125° .

Generally, the fit is around ~ 4 for all categories other than IV, X, and XII. There are very poor fits for categories X and XII, though these categories have anomalous readings in other analyses too. Other than these two categories, the errors are small.

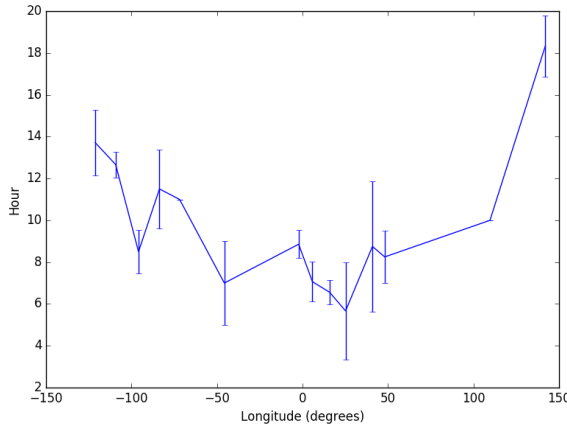


Figure 4.13: Peak hour of diurnal shift

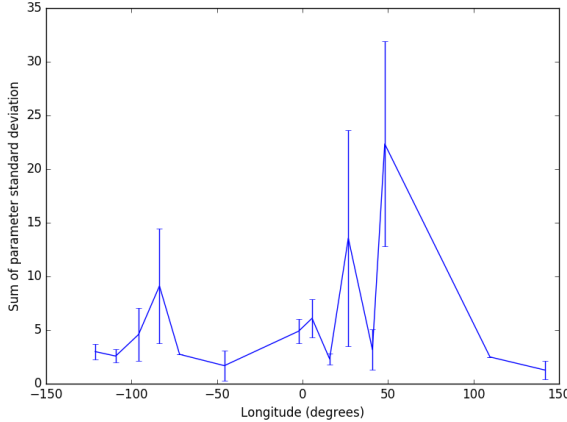


Figure 4.14: Fit of diurnal shift to an optimal sine function

4.5 Discussion

4.5.1 Latitude analysis

Mean, maximum & minimum hourly count

The mean does not appear to correlate with the latitude, but this is expected. Though the aim of this analysis was to determine if there are especially good locations for meteor detection, the reality is that on average, most places will be of the same quality for meteor detection.

It is not necessarily expected that the minimum *isn't* 1, though the reason is likely that most observers in the category *do* have a minimum of 1, but a few observers don't, which changes the mean min-

imum. This is a reasonable explanation, since the only categories that don't have a mean minimum of 1 have the largest sample sizes. Larger variations in maximum are expected. The maximum has no limit (theoretically) though the minimum cannot be below 0, so variation in minimum is limited but this is not the case for maximum hourly detection counts.

Skewness

The positive skewness is expected. There is likely to be more positive skew than negative, so on average it will be positive. Though most values are positive, they are all close to 0. This suggests that the distribution of meteor counts is symmetric.

Standard error

There appears to be, on average, a small amount of variation in hourly counts. This was not expected: often counts may vary widely across the course of a day, though the range over which the variation takes place is apparently small enough that the standard error is not large.

Diurnal shift

Correlation between latitude and the peak hour of an observer's diurnal shift is not expected, and this is reflected in the results. There is no apparent reason why the diurnal shift would vary with latitude, as discussed in chapter 3.

4.5.2 Longitude analysis

Mean, maximum & minimum hourly count

There is no expectation for a correlation between the mean and the longitude. There is a large variation in the results, though without an analysis of location based on latitude *and* longitude, there is no way of knowing if the increased mean hourly detection counts are a result of the location or an observer's detection system.

Skewness

Similar to the latitude analysis of skew, there is less grouping around 0 than expected. However, a slightly positive skew is not anomalous: counts will trail off towards larger numbers, but will never be below 0, giving a slightly positive skew.

Standard error

The large increase in standard error for categories X and XII are obscure. This increase could be due to the location, but most likely it is a result of the set up of the observers in the sample. This would explain the anomalous results, since the low sample sizes of 5 and 4 respectively would allow for a large variation due to a single observer's counts.

Diurnal shift

The apparent correlation between longitude and peak hour of diurnal shift is discussed in detail in chapter 3. It is an expected result based on the model for diurnal shift.

4.5.3 Improvements

Percentiles

Analysing the maximum and minimum hourly detection counts can only reveal a certain amount of information. It does give *some* indication towards the distribution of hourly counts, but taking quartiles, or 90th and 10th percentiles, will give more indication. The maximum may be extremely large, but there are no other values similar to it for a given observer, in which case the 90th percentile would reveal a lot more about the distribution. Similarly, the minimum is likely to always be 0 or 1, which does not provide much information, whilst the 10th percentile would indicate how many hourly counts are this small.

Joint latitude & longitude analysis

Whilst analysing latitude and longitude individually reveals, or thwarts, correlations, it is not as valuable as a joint analysis. This could be represented using a 3D plot, and would indicate much more clearly hotspots for meteor detection, and may reveal correlations that are not solely between latitude and longitude, but a correlation between the two.

4.6 Conclusion

There does not appear to be a large degree of correlation between most data characteristics and latitude or longitude. There appears to be a correlation between peak hour of diurnal shift and longitude, as expected based on the models discussed

in chapter 3. There are clearly anomalous readings for some results, namely standard error (longitude) and minimum hourly detection count (latitude). Likely explanations for this are low sample sizes. Further work, focusing on longitude and latitude, may clarify some results, indicating which apparent trends persist and which are anomalous.

Chapter 5

Temporal Variation of Radar Counts & Data Characteristics

Abstract

I present a study of the variation through time of radio meteor detection counts and characteristics of observer data. Results indicate a significant increase in radar counts between 2005 and 2011. I expand on previous research by Lindblad [4] and Bumba [1], providing these results which support their hypotheses of correlation between radar counts and solar activity. I also find an increase in meteor counts towards the middle of the year and discount day-night variation as a cause of increased counts.

5.1 Overview

In this chapter I investigate temporal variations in meteor detection count over time. There are many patterns that arise in meteor detection: diurnal shift over the course of a day, and showers causing variation over the course of a year. These variations can occur because of a variety of factors. In chapter 3 I have investigated the cause of diurnal shift, in chapter 7 I have investigated meteor showers. In this chapter I will analyse the variation of counts on a diurnal, monthly and annual scale. Knowledge of the variation seen in meteor detection may help to improve methods such as Zenithal Hourly Rate (ZHR); by providing a better understanding of the background detection counts, normalising data to investigate meteor showers can become easier. See chapter 7 for more on ZHR. Of significance is a comparison between these results and other analyses of temporal variation, but for visual detection: will radio detection be more influenced? Are the same variations seen? This analysis will demonstrate whether any variation is a worldwide phenomenon since the data set includes observers

from across the globe.

5.2 Literature Review

Lindblad (1968) [4] provides a similar analysis on long-term variation in meteor radar rates, as well as echo amplitudes. In this paper it is seen that the echo amplitudes correlate with the electron line density, indicating an influence from the solar wind. It is also observed that long-term variation in radio meteor detection count can be explained qualitatively by a variation in atmospheric density in the region where most meteors burn up, which itself is related to the solar cycle. During solar minimum, the shortest ionisation trails are seen, as well as higher electron line densities, suggesting that meteor echo signal strength will be greater at solar minimum.

Bumba (1948) [1] calculated the yearly rate of meteors as a function of position in the solar cycle, demonstrating that there is an inverse relationship between solar activity and detection counts: counts are maximised when solar activity is at a minimum.

5.3 Methodology

There are two main analyses.

5.3.1 Data characteristics

The first is an analysis of the variation over time of characteristics that summarise the data, specifically 4 values. (Note that these are the same as chapter 3 and 4, other than the mean, minimum and maximum values which are not included in this analysis). The standard error of all data for the observer is taken, which indicates how much the data varies. A lower value indicates that the same detection count is generally seen, and a larger value indicates that the detection count varies erratically. The skew also indicates the distribution of the detection counts. A positive skew indicates that the detection counts trail off towards high values, whilst a negative skew indicates that the distribution is ‘steeper’ for higher values, suggesting that there is a limit to the detection counts. The last two values are the peak hour of the diurnal shift, and the fit to an optimised sine curve for the mean detection counts over each hour of a day. This is calculated by averaging the values for all data for a given hour after midnight. A sine curve is then fit to this, in the same process as chapter 3, giving a sine function of the form $N = A \sin(\omega t + \phi) + \mu$ where N is the detection count. The calculated ‘fit’ is the sum of the standard deviations for A , μ , and ϕ . ω is assumed to be $\frac{2\pi}{24}$ so that the shift has a period of one day. These 6 values will be calculated for each observer, then the mean is recorded for all data for each month of each year.

5.3.2 Detection counts

The second analysis is of the mean hourly detection counts for all observers in the sample, over various scales. The scales being considered are daily, monthly and yearly. For yearly the mean will be taken over the entire year, as well as each month in a year, to give a higher resolution of the variation. A similar analysis, on the yearly scale, will be completed which uses data solely from the night-time, or day-time (for the location of the observer).

Location	Nº observers
Europe	220
North America	37
Asia & Australia	12

Table 5.1: Sample sizes for location categories

5.3.3 Analysis by location

Each of the above analyses will be repeated for data from all observers around the world from the RMOB data set, as well as specific locations, namely observers from Europe, Asia & Australia, and North America. The sample sizes for observers in each location category are shown in table 5.1.

5.4 Results

5.4.1 Data characteristics

Standard error

From figure 5.1 it is clear that the standard error is relatively small, and does not vary a great deal long term. There are short-term anomalies, for example in 2000 and 2008, for observers located in North America, and in 2005 for observers located in Europe. There is a clear increase in standard error for all categories from 2005 to 2011. The variation within each year does not appear to be periodic.

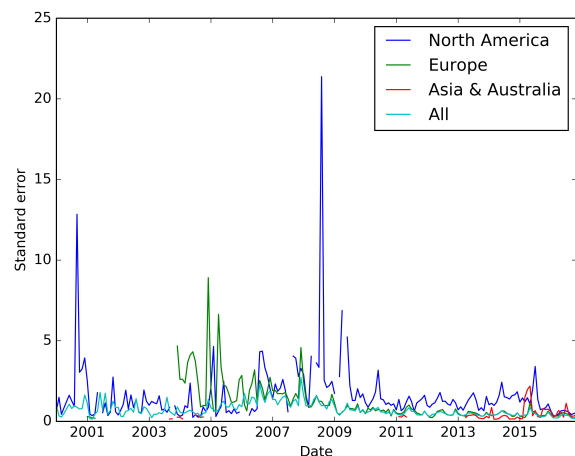


Figure 5.1: Variation of standard error

Skewness

There does not appear to be a long term trend. The skewness is generally larger than 0, however it varies by ~ 1 , around 2000. This variation decreases over time, and the skewness appears to be closer to 0 for years 2005 onwards. There are anomalous results, but they are short term. For observers located in Europe, the skewness dips below 0 around 2005–2011 before fluctuating around 0 from 2011 onwards. This is the same for all categories: the values fluctuate around 0 between 2011 and 2015.

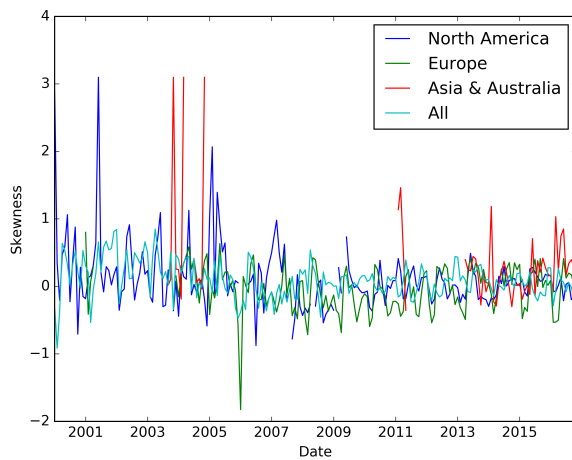


Figure 5.2: Variation of skewness

Diurnal shift

Between 2003 and 2007 there is a large amount of variation for observers in both Asia & Australia, and North America. Towards more recent years, the variation is much smaller for all categories. The overall trend is not clear due to the large variation. Mostly, each category appears to fluctuate around certain values. For observers in Europe, this is ~ 6 , in Asia & Australia the values fluctuate around ~ 18 , and in North America, around ~ 12 . During the periods with the most fluctuation in figure 5.3, the sum of the parameter standard deviations, indicating how well a sine function fits the data, is greatest. The mean fit, across all observers, is relatively low throughout the years available, however there is again a noticeable increase between 2005 and 2010, which fits in with increases & decreases in other analyses. The fit is closer to 0 in recent years, for all categories other than North America,

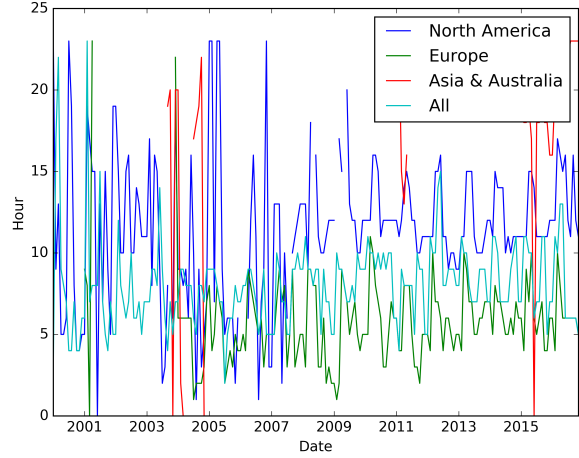


Figure 5.3: Variation of peak hour of diurnal shift

though this category does decrease too.

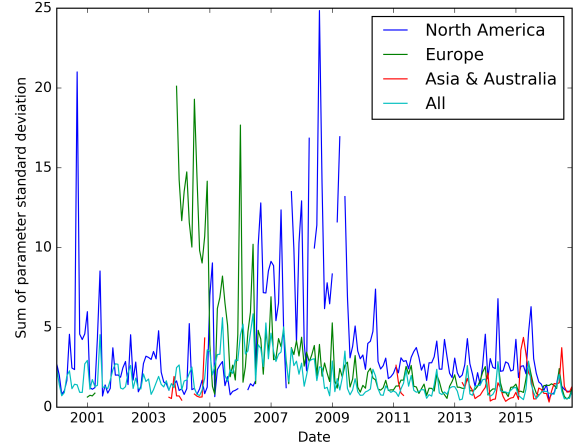


Figure 5.4: Variation of fit to optimal sine function for diurnal shift

5.4.2 Monthly scale variation

The variation over the course of a month is shown in figure 5.5. There is no overall trend throughout a month. There is no overall increase or decrease, though there is a slight increase around the 13th day in the month.

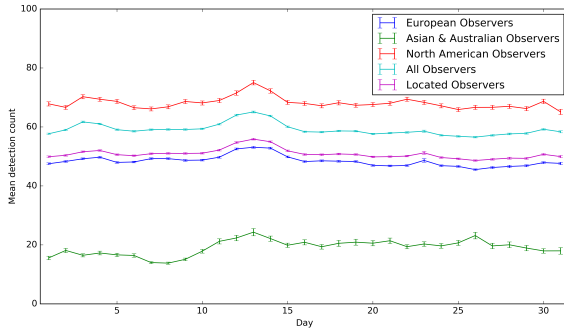


Figure 5.5: Variation in mean hourly detection count over a month

5.4.3 Annual scale variation

There is a clear increase from the beginning of a year to the end, for all categories other than Asia & Australia. From January to February, there is a small decrease, followed by an increase until June. This is followed by a small decrease of ~ 10 detections an hour, until August. The mean hourly detection count then remains roughly constant until the end of the year. This is the same for all categories other than Asia & Australia. For this category, there is an increase in April and May, and then a decrease and a constant hourly count for the rest of the year.

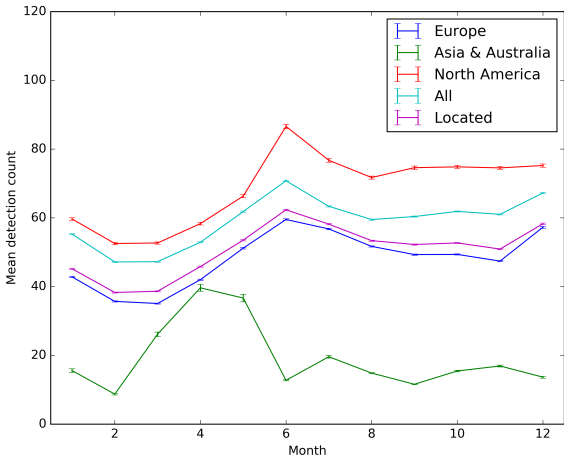


Figure 5.6: Variation in mean hourly detection count over a year

5.4.4 Variation since 2000

Between 2003 and 2011 there is a dramatic increase in the mean hourly detection count across an entire year. This increase is on the order of ~ 2 times, from ~ 60 to ~ 120 . This increase is out of phase by 1 year for the North American category. Once the count returns to ~ 60 , it remains there from 2011 to 2016. There is no data available for the Asia & Australia category for the maximum period so it is not known if the same increase is seen, however the category containing observers from the entire world exhibits the increase. Whilst the North American category has another peak in 2003, the standard error is much larger. Figure 5.8

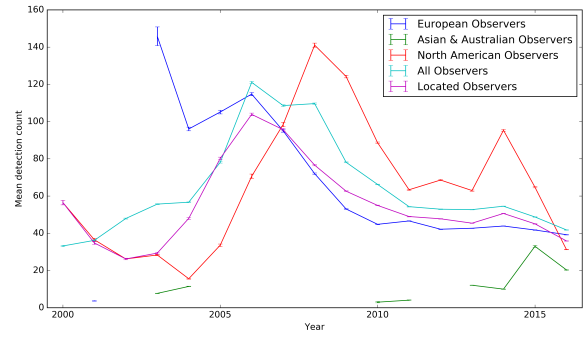


Figure 5.7: Variation in mean hourly detection count since 2000 by year

shows the same data as figure 5.7 but on a finer resolution: for each month of each year available. The same increase is seen as before, though it is clear there is much more variation between 2004 and 2011, as noted in section 5.4.1. It is clear from 2011 onwards, that there is a periodic variation each year, with a greater hourly detection count in the middle of the year.

Daytime vs. night-time rates

In light of the correlation between the solar minimum and the maximum detection counts, I carried out a paired t-test to determine if there is a significant difference between the mean hourly detection counts when considering only day-time values, and night-time values. There is no significant difference between day-time and night-time (1% significance level).

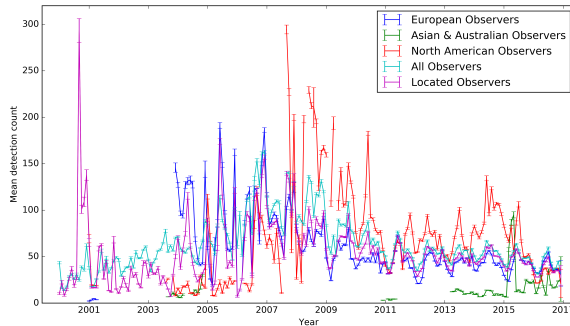


Figure 5.8: Variation in mean hourly detection count since 2000 by year and month

5.5 Discussion

5.5.1 Data characteristics

Standard error

The low variation shows that there are not large changes in hourly detection counts. This implies that influences from meteor showers do not greatly increase or decrease the detection counts, at least on a degree that would cause great variation. The increase from 2005 to 2011 agrees with figure 5.7, where the variation greatly increases during the maximum in detection counts. The influence of a solar minimum, causing greater detection counts, supports this. With the absence of a strong solar wind, variations in the number of meteors are likely to have more effect.

Skewness

It is expected that the skewness fluctuates around 0, primarily above 0. There will be an abrupt end in the distribution of possible detection counts since they cannot be negative, whereas there will be a tail towards large counts since there is (theoretically) no limit.

Diurnal shift

I provide no explanation for the large amount of variation in the diurnal shift peak hour for earlier years, towards 2000. In more recent years, the variation is less severe and the peak hour fluctuates around values that are expected from chapter 3. There is a worse fit during the years where there is a maximum in detection counts, possibly

because, with the greater detection counts, the diurnal shift has less influence on the total counts, meaning there is a worse fit for a sine function.

5.5.2 Monthly scale variation

It is expected that there is no overall trend over the course of a month. Any variation on this scale could potentially be caused by the moon, though it is unlikely that it would have an impact, and this is seen in the results. The small increase around the 11th–14th day of the month may be caused by a large shower, such as the Perseids, which causes such an increase in counts that it influences the mean across all months.

5.5.3 Annual scale variation

The increase in the middle of the year may be due to an increased number of meteor showers, or some other phenomenon. This increase can likely be considered part of the summer, since most observers in the sample are in the Northern Hemisphere. The low standard errors suggest that there is a clear periodic increase, and on the order of ~ 20 counts an hour. The Asia & Australia exhibits an increase, but two months earlier, and it does not persist for the rest of the year as other categories do. In chapter 3, it appears from an analysis of fit between a sine-curve and a given observer's data that the background detection rate increases between 2005 and 2011. This result, and that presented in this chapter, appear to agree. I do not put forward any explanation for this increase; further investigation is required. However, I should note that this increase in the middle of the year could be due to our position relative to the Sun, or other planets (Jupiter often ‘sweeps’ up debris) or simply fewer meteor showers. A good way to test this would be to remove meteor showers from the data and observe if the same increase is present.

5.5.4 Variation since 2000

The increase centred around 2007 is significant. The maximum of the hourly detection counts occurs between 2006 and 2008, whilst the solar minimum occurs in 2009: however the sunspot number is not much larger than this from 2006, as can be seen in figure 5.10. This correlation (as well as a

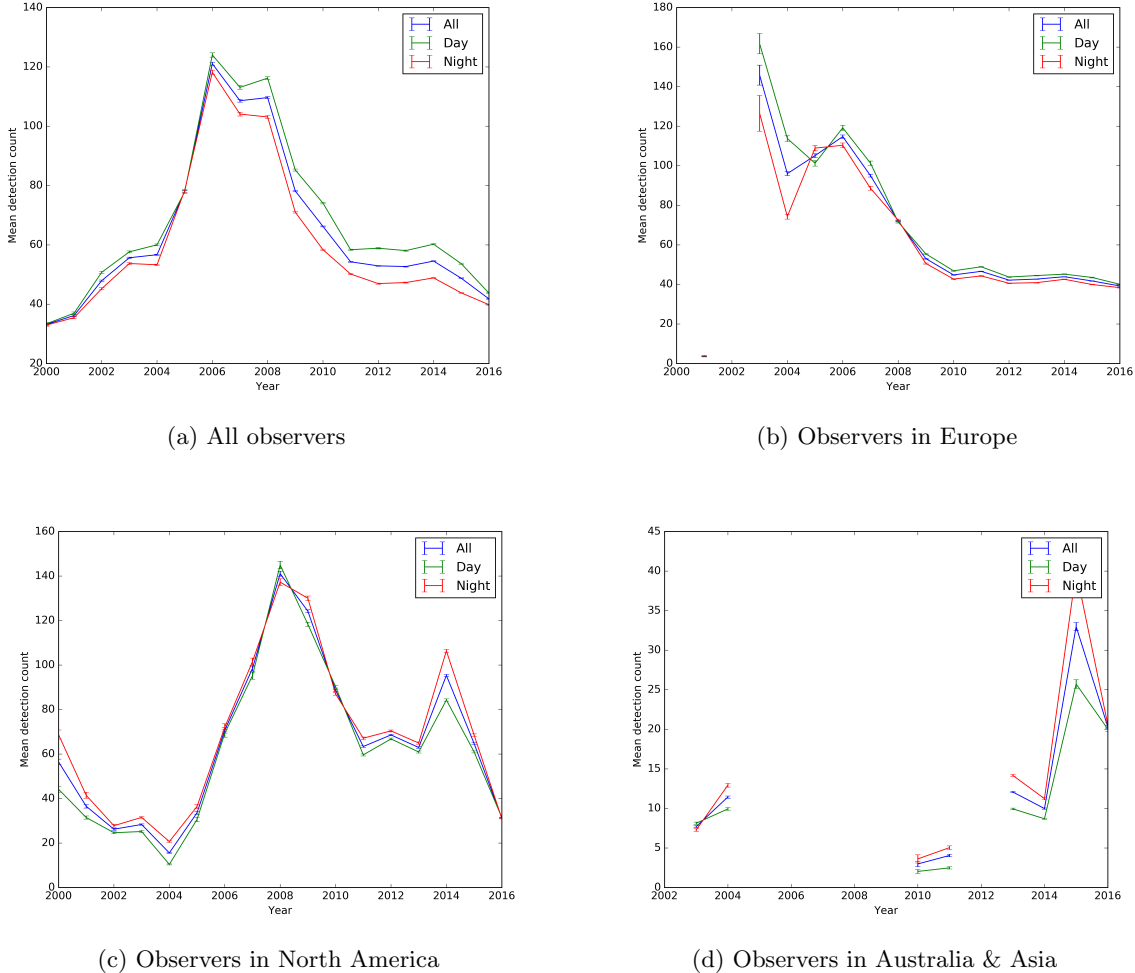


Figure 5.9: Daytime vs. Night-time hourly detection counts

slight phase difference of 1 or 2 years) between solar minima and meteor maxima is noted in other articles [4]. That the solar cycle has an impact on meteor detection rates is not unexpected. The solar cycle influences heavily the solar wind and electron density, which will have a large influence on detection rates, especially for radio meteor detection.

Daytime vs. night-time rates

The fact that there is no significant difference between day-time and night-time counts seems to disagree with other studies. However, this simply rules out an influence from the Sun being above the horizon, or not. This does not discount the influence of

the solar wind, since the change in electron density is not on only one side of the Earth. Thus any increase caused by the solar wind would not cause a significance difference between day-time and night-time counts. Theoretically, the peak hour of diurnal shift occurs at Sunset, so any influence will be uniform between day and night, so this can be disregarded.

5.6 Conclusion

I have found a significant increase in hourly detection counts between 2005 and 2011. The increase correlates well with solar activity, which sup-

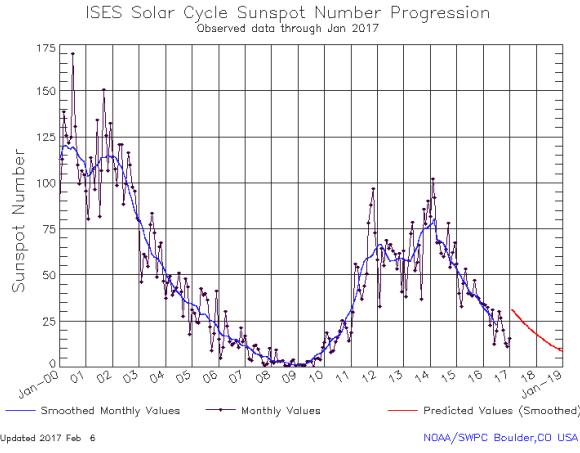


Figure 5.10: Solar cycle sunspot number over time [15]

ports hypothesis from Lindblad and Bumbda, as cited in section 5.2. There is no basis to reject the hypothesis that the day-time and night-time hourly detection counts are different (1% significance level), indicating that there is no influence on detection counts that varies over a single day's time frame. The results also show an increase in the middle of the year, which I provide no full explanation for. Further work on a hemispherical analysis may provide more information on this. A combination of a temporal and spacial analysis may also provide more information, since the two ‘dimensions’ of variation often work in conjunction with one another.

Chapter 6

Antenna Data Characteristics

Abstract

In this chapter I study the effect that antenna type has on the data produced by said antenna. This is done through an analysis of key characteristics describing important qualities of the data at hand. I find that, though there is variation between the differing types, there is no clear advantage for any of the considered antenna types. However, I also find that there are some indications as to which antenna type receives the best detection counts which may influence which antennas are used for future radio detection stations.

6.1 Background

Radio meteor detection can use a variety of different antenna types. There are 12 main types used in the RMOB data I am using. Yagi antennas are overwhelmingly the most popular, followed by dipole antennas (see figure 6.1). Each antenna

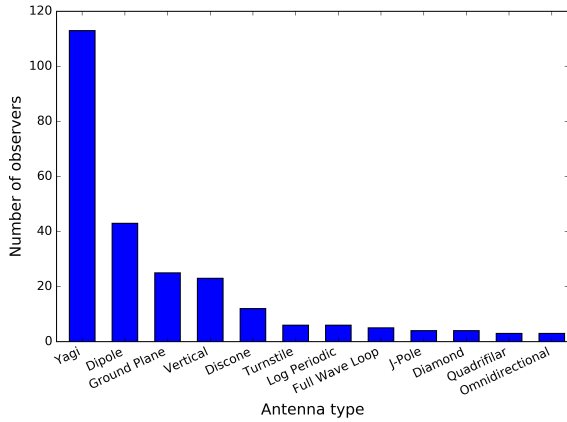


Figure 6.1: Antenna usage in RMOB data

type has its own merits and cons, but that is a discussion for another report.

6.2 Methodology

6.2.1 Selecting authors

There are 12 antenna types that will be analysed. In order to carry out the analysis, the observers must be split into groups for each of these types. This was done through manual selection: displaying the antenna type of each observer (if it has one), and choosing which type this antenna is, through a Python program. Any unknown types were declared as miscellaneous. These categories were then saved to their own file.

6.2.2 Analyses

The analysis focused on 6 values, aimed at summarising and describing the detections made by the observers in each antenna category. Two of these values are the mean and maximum of all data collected by each respective observer. The minimum is of little importance, since the value will almost always be 0 or 1. These indicate the typical detection counts for the observer. The standard error of the same data set is also taken, which indicates how much the data varies. A lower value indicates that the same detection count is generally seen, and

a larger value indicates that the detection count varies erratically. The skew also indicates the distribution of the detection counts. A positive skew indicates that the detection counts trail off towards high values, whilst a negative skew indicates that the distribution is ‘steeper’ for higher values, suggesting that there is a limit to the detection counts. The last two values are the peak hour of the diurnal shift, and the fit to an optimised sine curve for the mean detection counts over each hour of a day. This is calculated by averaging the values for all data for a given hour after midnight. A sine curve is then fit to this, in the same process as chapter 3, giving a sine function of the form $N = A \sin(\omega t + \phi) + \mu$ where N is the detection count and t is the hour. The calculated ‘fit’ is the sum of the standard deviations for A , μ , and ϕ . ω is assumed to be $\frac{2\pi}{24}$ so that the shift has a period of one day. A comparison is made of these 6 values for each antenna type.

6.2.3 Sample sizes

Sample sizes for each antenna category are shown below.

Antenna	Nº observers
Diamond	4
Discone	12
Full wave loop	5
Ground plane	25
J-pole	4
Log periodic	6
Omni	3
Quad	3
Turnstile	6
Vertical	23
Yagi	113

6.3 Results

6.3.1 Mean & maximum

Figure 6.2 shows the result for the mean and maximum counts for each hour, averaged for each respective antenna type. There is no clear difference between the means, as shown by the error bars, which show standard error. The largest mean

is for a Turnstile antenna, though this is likely due to a single observer with a large detection count, and this is supported by the large standard error. There is also no significant difference in the maximum values. The most extreme (both large and small) maximum counts have larger error bars, which suggests that there are only a few observers which have these maximum counts out of all those in the antenna category.

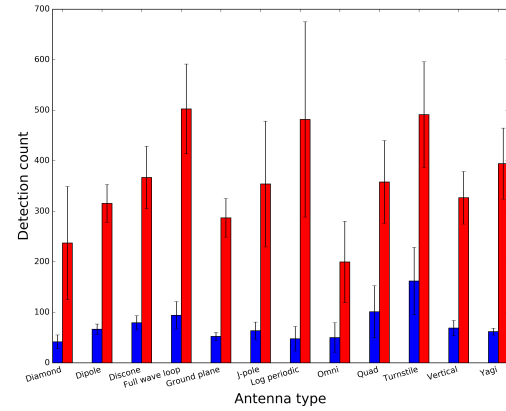


Figure 6.2: Mean and maximum hourly detection counts (maximum count in red, mean in blue)

6.3.2 Standard error

Figure 6.3 shows the results for the mean standard error of the hourly counts for each antenna category. The most extreme values have the largest error bars, suggesting that this is because there is a small sample size. However, the turnstile, vertical and j-pole antennas have the largest standard errors, suggesting these antennas produce data with the most variation. Log periodic, ground plane, full wave loop and diamond antennas have the lowest standard error suggesting the lower variation of the data.

6.3.3 Skew

From figure 6.4, it can be seen that log periodic, vertical and Yagi antennas have the largest positive skew, with turnstile, discone and full wave loop antennas with the largest negative skew. Generally, a positive skew is expected since the data should

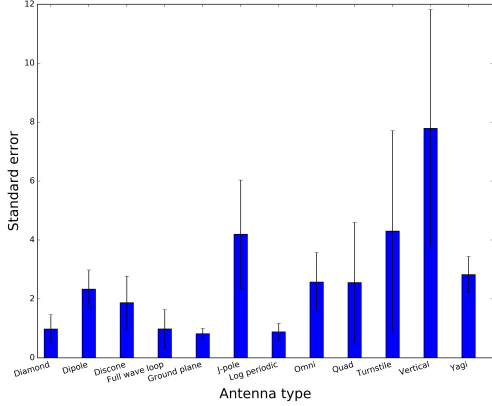


Figure 6.3: Variation of hourly detection counts

trail off towards larger counts, whereas no counts are valid below 0, so there is a steeper end to the distribution of data. This is not seen in the data. The skewness values for each antenna category are relatively evenly distributed around 0. 5 of the categories have a standard error in the skew that is larger than the skew itself, suggesting that these values are not significant and cannot be considered completely valid.

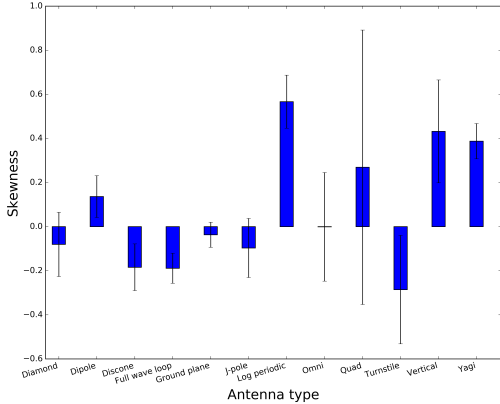


Figure 6.4: Skewness of hourly detection counts

6.3.4 Diurnal shift

The results are relatively evenly distributed around a peak hour of 9: however, as found in chapter 4, this is most likely due to the geographical

location where the antenna is used. Based on this, it is likely that ground plane, omni, quad and turnstile antennas are mostly used in Europe, whilst full wave loop, J-pole and diamond antennas are used mostly at latitudes $\sim -180^\circ$ and 180° .

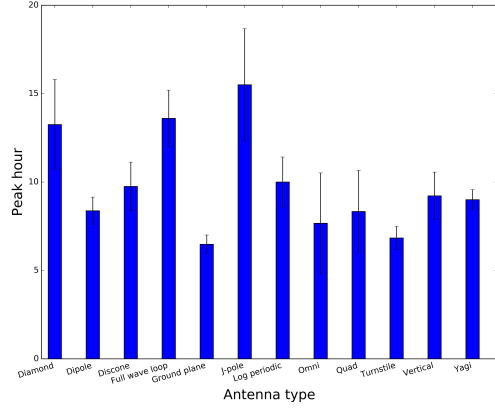


Figure 6.5: Peak hour of diurnal shift

The larger results for J-pole, quad, turnstile and vertical antennas suggests that these are not as influenced by diurnal shift. However, these categories have much larger standard errors than other categories, suggesting that there is simply a low sample size. Vice versa, ground plane and log periodic antennas have much better fits to a sine curve, implying the antennas are more influenced by diurnal shift.

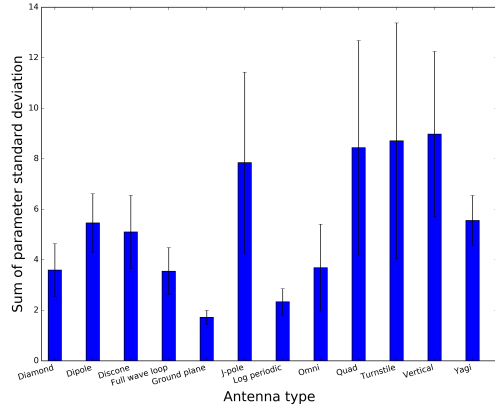


Figure 6.6: Fit to optimal sine function for diurnal shift

6.4 Discussion

6.4.1 Mean & maximum

There is no clear trend for an antenna which produces data which, on average, has greater hourly counts. This is expected. Were there an antenna that was particularly good at radio meteor detection, it would likely be used widely. Equally, if there was an antenna that produced particularly poor data, it would not be used at all. The standard errors, for all categories, range across ~ 20 counts an hour. This is substantial, and suggests that there is little agreement between characteristics of data for observers that use the same antennas.

6.4.2 Standard error

For some categories, the mean standard error is much larger. However, these categories have greater errors. Diamond, full wave loop, ground plane, and log periodic antennas appear to produce data with the lowest amount of variation. The implication is that the antennas are poor at detecting meteors, so there will be little variation in the counts. However, comparing these categories with figure 6.2, they are the lowest categories (other than full wave loop), but not significantly lower than others.

6.4.3 Skew

Log periodic, vertical and Yagi antennas all appear to produce reasonably positively skewed data. The same extremity is not seen for a negative skew. Other than vertical antennas, the error is not too large, indicating that there is *some* correlation. A lack of correlation with other properties indicates that this is an anomalous result. However, further investigation may yield this to be false.

6.4.4 Diurnal shift

Variations in the peak hour of diurnal shift are likely due to location, as discussed in chapter 3 and 4. However, most antennas appear to produce data with peaks around hour ~ 9 . Errors for all categories are substantial, indicating little agreement

within each category. Ground plane and log periodic antennas appear to produce data that fits a sine-function very well, indicating a greater periodicity in the data than other antennas. The poorest fits have large standard errors, indicating that these values are of little validity.

6.4.5 Improvements

Location From previous chapters, it is known that the location where data is collected will influence the results. Because of this, simply grouping together observers who use the same antenna may not give an accurate reflection of the data characteristics unless the data is somehow normalised so that location has no effect. The simplest way to do this is to include more observers, and then analyse the antenna categories. When comparing these results, the location can be factored into any conclusions, removing the influence that location has on the data.

Yagi n-element analysis

In my analysis I have grouped *all* Yagi antennas into the same category. An analysis based on the number of elements on the antenna within the yagi category may indicate if there is an optimal number of elements for meteor detection, as well as the effect of different numbers of elements on the characteristics of the data.

Coefficient of variation

Instead of using standard error of the hourly detection counts to indicate the variation of the data, it may be better to use the coefficient of variation, c_v , defined as $c_v = \frac{\sigma}{\mu}$ where μ and σ are the mean and standard deviation of the data respectively. This gives a better reflection of the variation as instead of factoring in the sample size, it factors in the mean. This is an improvement since the degree of variation is no longer proportional to the mean, giving no skew favouring lower means.

Percentiles

As part of the data characteristics analysis, I used the maximum count to help summarise the data. This is not a very useful summary value to make, since the maximum itself holds little value.

What would indicate the distribution of data better is a value such as the 90th percentile. This may give a better reflection of the data that an antenna produces.

6.5 Conclusion

There is no clear correlation between any characteristics and the antenna types. However, J-pole, log periodic and turnstile antennas consistently have the most extreme values. However, the extremes for these antenna types do not necessarily imply the same characteristics of the data. Log periodic antennas appear to provide consistently positive-skewed data. Turnstile antennas appear to provide the largest detection counts. A consistent theme throughout the results are large errors, suggesting large variation within each antenna category, implying little correlation between the given antenna type and the characteristic under consideration. Greater sample sizes, as well as isolation of other variables (location, time) may reveal more correlation.

Chapter 7

Zenithal Hourly Rate Validity for Radio Detection

Abstract

I present an improved formula for calculating Zenithal Hourly Rate (ZHR) and an analysis of its validity for radio meteor detection. Beyond this, I assess the implications of the resultant ZHR for antenna field of view, meteor shower population index and stream density. The formula, with modification is valid, and the results agree well with visual results. There are clear improvements that can be made, though as a first approximation the formula is adequate.

7.1 Background

Zenithal Hourly Rate (ZHR) is a measure of the activity of a meteor shower. The value indicates how many meteors an observer can expect to see, assuming optimal viewing conditions, with the meteor shower radiant at the observer's zenith (directly overhead).

7.2 Literature Review

7.2.1 Calculating ZHR

A formula already exists for calculating the theoretical ZHR from known data and conditions [5]. The formula (7.1) depends on four correction factors.

$$ZHR = \frac{\overline{HR} \cdot F \cdot r^{6.5-m}}{\sin(h)} \quad (7.1)$$

The hourly rate is given by $\overline{HR} = \frac{N}{T_{eff}}$, N is the number of meteors observed, and T_{eff} is the effective observation time of the observer. This corrects the number of meteors detected such that

it is an hourly rate.

The correction for the field of view, F , is given by $\frac{1}{1-k}$ where k is the percentage of the observer's field of view that is obstructed.

The correction factor for limiting magnitude is given by $r^{6.5-m}$, where m is the limiting magnitude of the observer. This corrects the value such that it is representative of the ZHR when the limiting magnitude is 6.5. The value of r itself is the population index: a measure of the magnitude distribution of the shower. For each increase by 1 in magnitude (bearing in mind that a greater magnitude is a lower value), the number of meteors you would expect to see increases by r .

The final correction factor is for the altitude of the radiant above the horizon, measured as an angle. This is effectively $\frac{\pi}{2} - z$ where z is the zenith distance in radians. The radiant is the observed point of origin for all meteors in the shower. This correction factor is given by $\sin h$ where h is the angle from the horizon to the radiant.

7.2.2 Meteor shower information

The International Meteor Organisation (IMO) provides a list of “meteor shower calendars” [19]. These contain a list of notable meteor showers, with information on these showers including the active range (period in which the shower produces visible meteors), the date of its maximum, the expected ZHR, radiant co-ordinates (in right ascension and declination), and finally the population index. This calendar will be the source of my data for visual observation data, and will provide the information from which comparisons can be made with the radio observation data.

7.3 Methodology

7.3.1 Assumptions

The following assumptions are made in my calculations.

- The receiving antenna is active for the entire period where data is available.
- The antenna detects meteors across the entire sky.
- Detected meteors are travelling tangential to Earth’s surface.
- The shower meteors are incident uniformly in all directions around the radiant.

7.3.2 Formula modification

The formula [5] for ZHR has a number of issues that cause inaccurate results. In order to use the formula in my analysis, these errors must be corrected.

Inaccuracy of radiant height correction

Problems

Perhaps the largest error is that of the radiant height correction. The correction assumes a sine function of the angular radiant height, which varies (with $-\frac{\pi}{2} \leq h \leq \frac{\pi}{2}$) between -1 (for $h = -\frac{\pi}{2}$) and 1 (for $h = \frac{\pi}{2}$). This creates a number of issues: when the radiant approaches the horizon, h approaches 0, as does $\sin h$. This means that the correction (which is $\frac{1}{\sin h}$) approaches ∞ . This is

clearly wrong. When the radiant approaches the horizon, the number of meteors observed doesn’t approach 0, and thus the correction should not approach ∞ . In other words, you do not see infinitely many meteors when the radiant is at the zenith compared to the horizon. Further to this, the use of a sine function simply means that there is *no* way a calculation can be made when the radiant is at the horizon — this should be possible. The sine function also results in a negative ZHR when the radiant is below the horizon. Clearly, you do not expect to see anti-meteors when the radiant is below the horizon.

Previous Solution Solutions to the issue with the radiant height correction factor have been studied previously [7]. In this article, a piecewise function is noted from Kresák [3] which uses a cosine function of the zenith distance (which equates to a sine function of the radiant altitude) down to 80° , and then uses another function which extends the domain of the model to $\sim 100^\circ$. The article itself puts forward a complex function which works over a similar domain. This is not a first approximation though, it is an attempt at an accurate function to describe the flux correction factor for a range of radiant altitudes. The article notes that there is a small, yet present, possibility of shower meteors for a radiant below the horizon, and the reason for this dramatically lower expected detection count is that the atmosphere shields the Earth from most of the debris, and only those travelling tangential to the Earth’s surface are detected. This may be applicable to visual observation, but radio detection almost relies on meteors travelling tangential to the Earth’s surface, so the radiant being below the horizon does not have such a dramatic effect. For this reason, I do not believe this is a useful replacement for the correction factor.

Solution

From a basic geometric standpoint, the number of meteors you expect to observe, varying with the radiant height, should depend on the proportion of a hemisphere (with the radiant at the pole) that is visible. Of course, this assumes that meteors travel from the radiant uniformly in all directions.

A wedge of a sphere has a curved surface area of $2\alpha r^2$, where α is the angle at the central axis of

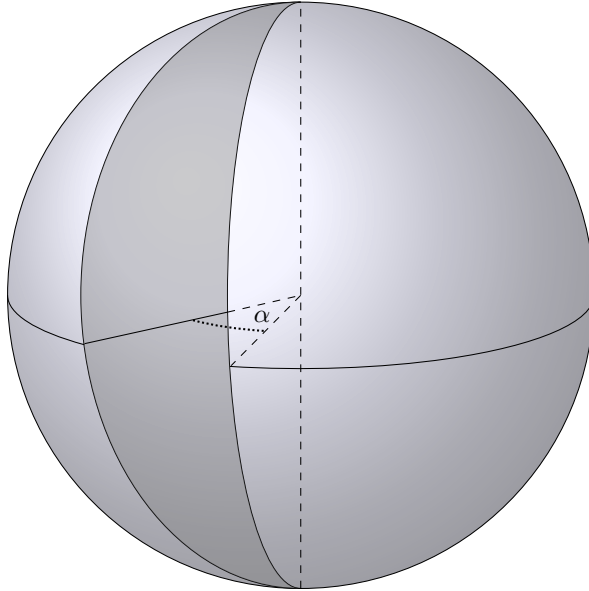


Figure 7.1: Spherical wedge curved surface area

the wedge (see figure 7.1). Thus, the proportion, p , of the hemisphere that is visible is $\frac{2\alpha r^2}{2\pi r^2} = \frac{\alpha}{\pi}$. For an angle h (the radiant height as an angular distance) varying between $-\frac{\pi}{2}$ and $\frac{\pi}{2}$, the proportion will vary between -1 and 1 (perhaps where the original sine factor came from). When the radiant is at the zenith, you would obviously expect to see the same number as if the radiant was at the zenith, so the correction factor, c , is 1 (see figure 7.2).

When the radiant is at the horizon, half the hemisphere is visible, so you would expect to see half the number of meteors at the zenith ($c = 2$), and when the radiant is directly below you (at the nadir) then you would expect to see no meteors (from the shower), since none of the hemisphere of the radiant is visible to you. Mapping the proportion linearly from $-1 < p \leq 1$ to $0 < \frac{1}{c} \leq 1$ yields $\frac{1}{c} = \frac{1}{2} + \frac{h}{\pi}$ for $-\frac{\pi}{2} < h \leq \frac{\pi}{2}$, where h is in radians. This satisfies the *expected* correction factor.

Population index limitations

The population index indicates the magnitude distribution of the meteor shower. For each extra magnitude of visibility, an observer would expect to see r times more meteors. This is true, but only up to a point. Without a limit on how far this model works, the implication is that this

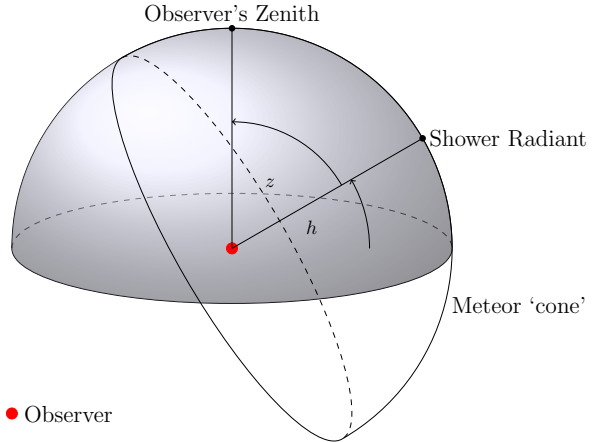


Figure 7.2: Diagram for derivation of radiant height correction factor. The shaded hemisphere is the observer's field of view.

power-law distribution carries on forever. Clearly this is not true: if limiting magnitude was (rather absurdly) 40, you wouldn't expect to see 1.1 trillion meteors (if $r = 2.0$). Thus the model is not applicable for limiting magnitude, $m > 6.5$, since the model that the magnitude distribution is of the form $N = N_0 r^m$ is no longer valid. The radio observation of meteors has a larger limiting magnitude than visual observation: meteors down to the size of a grain of sand, and smaller, can be detected. Thus the population index model is not applicable for radio meteor detection, unless the model is refined for larger limiting magnitudes.

Background detection count

In visual observation of meteors, the background level of sporadic meteors is rather low. However, for radio meteor detection, there is a much greater background detection rate and this will impact how accurate the ZHR is. A correction is required to remove the effect of any background detection rates. The calculation of this background rate is a chapter in itself. If the baseline is larger than any detection counts within the active range, the resulting ZHR will be negative, and this is not a valid result. A solution to this is to choose the minimum hourly detection count in the active range of the shower, but this is rather artificial, and often results in a baseline of 1 or 0. Instead, I have decided to calcu-

late the background hourly detection count by taking the mean hourly detection count for the lower quartile of all hours outside the active range of any meteor showers. This will result in some ZHRs being negative, but these results should be minimal and can simply be discarded.

Field of view correction

I will not include a field of view correction factor, since it is not possible to know exactly the field of view that each antenna has available, because it is not part of any data that an observer can upload to RMOB. This *should* have a reasonably large impact on the results, however the correction factor will be absent for all calculations so the error is the same everywhere (on average). In fact, the final results may allow the average field of view to be calculated.

7.3.3 Calculating radiant height

From the spherical law of cosines, we know that

$$\cos z = \sin \phi \sin \delta + \cos \phi \cos \delta \cos (\theta - \alpha)$$

where z is the zenith distance, ϕ is the observer's latitude, α and δ are the right ascension and declination of the shower radiant, and θ is the local apparent hour angle (an angular measure of local sidereal time, which effectively measures time against the stars rather than the Earth's rotation). Since $h = \frac{\pi}{2} - z$, $\cos z$ can be replaced with $\sin h$. This relates the radiant altitude to the longitude of the observer and the radiant's astronomical coordinates.

7.3.4 Calculating hourly rate

The hourly rate is given by the observed hourly rate (the data I actually have), minus the baseline hourly rate. This *should* be divided by the effective observation time, but since I am making the assumption that the antenna are receiving across the entire hour, then there is no need for this.

7.3.5 Analysis

Selecting observers In order to carry out the analyses, the observers had to be split into groups for each shower. This was done simply by checking which months each observer was active for, and

Shower	N° observers
Geminids	67
Leonids	61
Orionids	43
Perseids	39
Quadrantids	58
η aquariids	34

Table 7.1: Sample sizes for meteor showers

adding it to a given category if the observer was active during the shower. This selection was refined further so that an observer must be active for the entire peak date, and have no more than 12 inactive hours during the active period of the shower. The sample sizes for each shower are shown in table 7.1.

Comparison

My analysis of the ZHR will centre around a comparison between the summary statistics for the ZHRs from the hourly counts for the stored observers, and known values for the ZHRs for applicable years. The process of calculating the ZHR follows a simple process of calculating the correction factors, correcting the known hourly rate, and discarding any invalid values (e.g. negatives). The formula, after modification, is

$$ZHR = \frac{N - r}{\left(\frac{1}{2} + \frac{h}{2\pi}\right)}$$

where r is the background hourly rate, and N is the number of meteors detected for one hour. The error is given by

$$S.E. = \frac{ZHR}{\sqrt{N}}$$

This calculation will be done for each hour available, and then a mean will be taken. This process will be applied to three ranges of dates: the entire active period of the shower (for a given year), two days either side of the peak date, and the peak date. Once this has been calculated for all the available data in the given ranges, the mean and 90th percentile are recorded. These will then be compared to the known values from the IMO meteor shower calendar [19]. I am using the 90th percentile rather than the maximum ZHR since the maximum itself is of little worth to indicate the distribution

of ZHRs. A box plot for each year of each shower would yield the most information but would provide far too much data to consider at once, whereas the 90th percentile indicates the maximum clearly without producing the exact same result if, for instance, the maximum ZHR was the same across all three periods under consideration.

In order to assess the agreement between radio and visual ZHR, I use Pearson's Moment Correlation Coefficient (PMCC) to give a quantitative measure of correlation, indicating how well radio results reflect visual results.

Correction factors

The final results will then be used to estimate the average field of view across all observers whose data are used, as well as the average limiting magnitude. This is a rough calculation, and is likely to have a large uncertainty, but it gives an estimate towards the true values and is an interesting calculation to make. The formula for the field of view factor is

$$k = 1 - \frac{ZHR_{mean}}{ZHR_{exp}}$$

For the limiting magnitude,

$$m = \log_r \frac{r^{6.5} \cdot ZHR_{mean}}{ZHR_{exp}}$$

For each of these calculations, ZHR_{mean} is the calculated mean ZHR for the peak of the shower, and ZHR_{exp} is the maximum visual ZHR for the same shower and year. It is clear that a negative k will be the result when the mean ZHR of the peak is less than expected, and positive otherwise. Any negative values can be discarded. Equally, a limiting magnitude will be less than 6.5 if the mean ZHR of the peak is less than expected, otherwise it will be larger than 6.5. Values less than 6.5 can be discarded. This means that the correction factor that applies will either be for field of view, or limiting magnitude, not both.

7.4 Results

The full results are shown in appendix A. In this section, important results are noted. In graphs comparing radio and visual ZHRs, the results considering only the peak (indicated by a dot-dash

line) are the most important to consider, since these are for the same period as the maximum visual ZHR results.

7.4.1 Comparison

Geminids

Figure 7.3 shows the mean radio ZHRs for the peak period, peak \pm 2 days, and the entire active range compared to the maximum visual ZHRs for each year. There is no clear agreement between the two methods of assessing ZHR. The results for radio ZHR are lower than expected for all years other than 2012. However, given the radio ZHRs were adjusted by a certain offset, they may appear similar to the visual results.

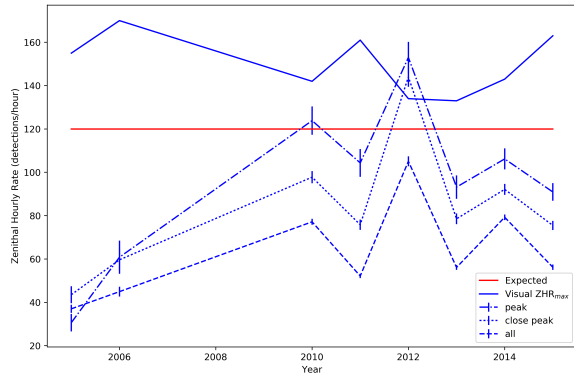


Figure 7.3: Geminids shower mean radio ZHR compared to visual maximum ZHR and expected ZHR.

It is important to note that the radio ZHRs are not dramatically different to the visual results. The visual ZHRs do not fluctuate more than around 20 detections an hour, and the radio results, whilst fluctuating more than the visual ZHRs, centre around a certain value in a similar way to the visual results.

Leonids

The results for 2007 are much higher than expected. Other than this year, the results are much closer to the visual ZHRs. The visual ZHRs fluctuate over a range of \sim 20, and (disregarding 2012) the radio ZHRs appear similar. A decrease is exhibited in the visual results towards 2016, and this is reflected in the radio results, indicating good agreement. Equally, the visual ZHR is lower in 2005 and

this is seen in the radio ZHR, too. 2012 stands out as an erroneous year, though there is a much larger standard error in the results (indicated by the error bars), suggesting either a low sample size or anomalous results.

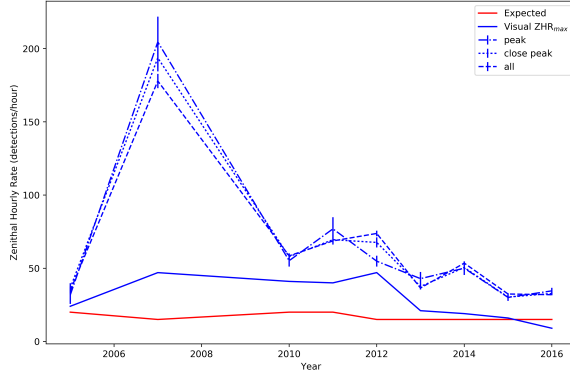


Figure 7.4: Leonids shower mean radio ZHR compared to visual maximum ZHR and expected ZHR.

The radio ZHRs are similar to the visual maxima though are greater, however the correlation between increase and decrease of the expected ZHRs and calculated ZHRs implies that the issue is simply a matter of a correction factor, e.g. field of view or population index (the leonid shower may have a large population index, indicating that with the higher limiting magnitude for radio observation, you detect more meteors).

Orionids

For all years where data is available, the calculated ZHRs are consistently greater than expected. However, the radio ZHRs follow a very similar form to the visual results: the results are larger in 2010 and 2011, decreasing in 2012 and 2013, followed by a slight increase up to 2016. The two sets of data agree with each other well.

The errors are similar for the considered years. This indicates a good agreement between the authors in the sample, which in conjunction with the similar forms indicates that the radio ZHR is a good reflection of visual ZHR. However, the radio results are consistently greater than the visual results.

Perseids

Year on year, similar results are seen. The radio

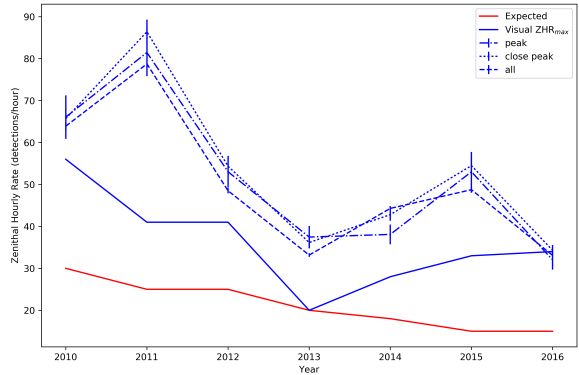


Figure 7.5: Orionids shower mean radio ZHR compared to visual maximum ZHR and expected ZHR.

and visual ZHRs are similar for the peak period throughout the years considered. A similar form is seen between radio and visual ZHRs. In 2010 a larger maximum visual ZHR is recorded, and the radio ZHR is larger, too. However, not as great as 2012, despite a lower visual ZHR. Anomalies like this are to be expected, and the more important detail of form appears to have good agreement between radio and visual. The maximum visual ZHRs are greater in 2012, 2013, 2015 and 2016, and this is reflected in the radio ZHRs, other than in 2016. Again, anomalous results such as this should be expected.

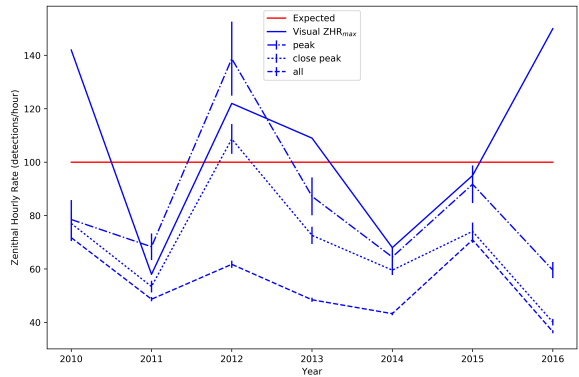


Figure 7.6: Perseids shower mean radio ZHR compared to visual maximum ZHR and expected ZHR.

Overall, the agreement between the radio and visual ZHRS for the perseid shower is good. The increases and decreases in visual ZHR between each

year are well represented by the radio ZHR results.

Quadrantids

The variation in the maximum visual ZHRs is reflected well in the radio ZHR results. In 2011 and 2012 the means for the peak are very close to the visual maximum. Whilst the remaining years are not as close to the visual maxima, where the maximum increases (2013, 2014), the mean ZHR for the peak increases, and then decreases for 2015 and 2016, as does the visual maximum.

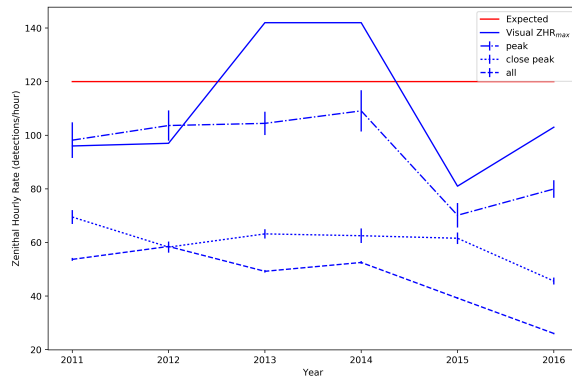


Figure 7.7: Quadrantids shower mean radio ZHR compared to visual maximum ZHR and expected ZHR.

The results for the peak ± 2 days, as well as the entire active period are much lower than the peak period. This change is not seen as clearly for the other showers that have been analysed. Not only do the results reflect the visual results well in form, but in value too. The majority of results for the radio ZHR on the peak day is similar to the maximum visual ZHRs.

η -aquariids

The results for radio ZHR match those for visual ZHR well. The maximum visual ZHR decreases from 2010 to 2012, and continue this trend at a lower rate to 2016, other than an anomalous result in 2013 which is much greater than other years. This trend is matched similarly by the radio ZHRs, other than the anomalous increase in 2013.

The radio ZHR results are of very similar value to the maximum visual ZHR for each year. Year on year changes are reflected well by the radio

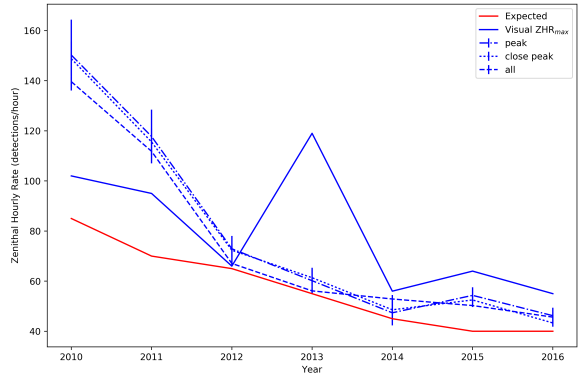


Figure 7.8: η -aquariids shower mean radio ZHR compared to visual maximum ZHR and expected ZHR.

results, though the standard errors are relatively large. This could be due to a low sample size, or simply disagreements between observers in the sample. However, the mean values correlate well with visual ZHR.

Correlation It is difficult to comment on how good the correlation is when taking into account all the previous results, so it is best to use a scatter graph of all results. Figure 7.9 demonstrates the correlation between visual and radio ZHR. The dotted line shows the line of best fit. It is clear from this figure that there is a correlation between radio and visual ZHR results. There are some anomalous results, but this is expected from any dataset. The correlation coefficient is $r = 0.458444$, with p-value of $p = 0.00175$, indicating there is a good correlation.

7.4.2 Correction factors

The results for the correction factors are shown in table 7.2. There is no field of view factor for the Leonids shower since there were no values larger than 0. Equally the Orionids field of view factor can be disregarded since the standard error is larger than the mean itself.

7.5 Discussion

7.5.1 Comparison

Peak

Frequently throughout the data the mean ZHR for the period of the peak is lower than the peak \pm 2 days. This indicates that the peak is in fact different to that used for calculating the ZHR. Alternatively, this could be due to a difference in the size of density throughout the meteor stream that causes each meteor shower. As the Earth moves through the stream, there may be smaller debris causing the shower, which would not be as easily noticed in visual meteor detection, but with radio detection's greater effective limiting magnitude, this is noticeable. This may also explain why in some showers, in some years, the mean ZHR decreases from the entire active range towards the peak, whereas some simply decrease for the peak compared to the peak \pm 2 days, but the mean ZHR for the peak is still greater than the entire active range.

In some results, there is a large increase from the peak \pm 2 days to the peak period. This indicates a shower with an intense peak, where the stream density increases dramatically on the peak day. The exhibition of this in the radio ZHR results indicate that it is a good measure of activity in a shower and can yield useful information.

Provided the data was adequate, it may be possible to estimate the true peak of a meteor shower. Analysing the mean, or 90th percentile, of the ZHR for a range of 24 hour periods, and selecting the largest values, should indicate which period contained the peak. This could, of course, then be focused down into 1 hour periods.

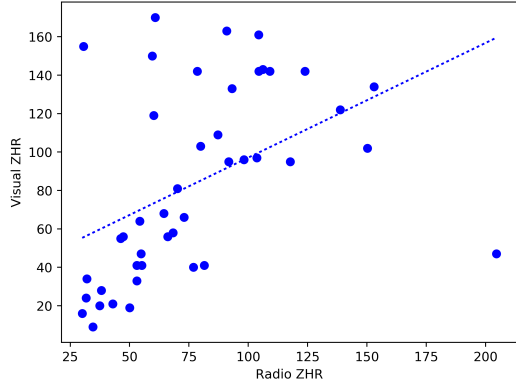


Figure 7.9: Scatter graph of visual and radio ZHR results. Visual ZHR is the maximum visual ZHR of the peak period, radio results are the mean ZHR of the peak period.

Shower	$m \pm S.E.$	$k \pm S.E.$
Geminids	6.63 ± 1.00	0.418 ± 0.0334
Leonids	7.29 ± 0.0563	0 ± 0
Orionids	6.96 ± 0.0382	0.0581 ± 1
Perseids	6.69 ± 0.0157	0.267 ± 0.0500
Quadrantids	6.56 ± 0.0209	0.214 ± 0.0140
η aquariids	6.77 ± 0.0551	0.240 ± 0.0424

Table 7.2: Limiting magnitude (m) and % obstruction (k) for each shower

Stream density

In the geminid shower especially, there is not a large amount of variation between each period for each respective year. This indicates that the debris density of the stream is more consistent than most streams. In the quadrantids shower, the opposite occurs. The variation between the peak and other periods is significant and this indicates that the stream density changes much more on the peak.

Variation correlation

In most showers, the variation in the maximum

visual ZHR is reflected in the calculated mean ZHRs. The trends in visual ZHR are reflected well by the radio results. This suggests that the formula used to calculate the data works well and is valid as a method of analysing shower activity using radio meteor detection. However, the difference between the maximum visual ZHRs and the means is still significant for some showers, indicating that other correction factors such as field of view and limiting magnitude still have an impact. The maximum visual ZHR is a better indicator for this variation than the expected ZHR, since the expected ZHR is only an estimate, whilst the maximum visual ZHR is a direct calculation from recorded data. The good correlation is supported by the result of $r = 0.458444$ and p-value indicating that, at the 1% significance level, there is a good correlation.

7.5.2 Correction factors

Field of view

The values for k are used to calculate the field of view correction factor. The values are not as expected. Typically, 50% or less of the sky can be seen with any normal sized ($\approx 5\text{m}$) receiver. For example, see figure 7.10 which shows the beam of a Yagi antenna. Clearly, the results do not agree with this beam, much more than 40% of the view is not seen. (I use a yagi antenna as an example since it is the most popular antenna type). The closest value to 50 % is for the geminids shower, however this is still not close. It should be noted that this is an estimation: in conjunction with other factors, values may be closer to expected.

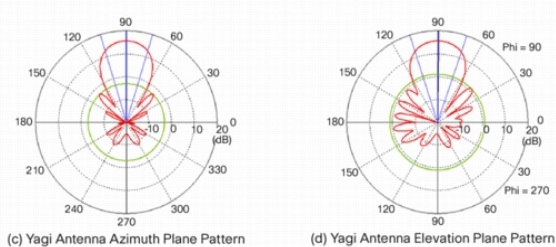


Figure 7.10: Yagi beam diagrams [11]

Limiting magnitude

The limiting magnitudes are not as high as expected for radio detection. This demonstrates the fact that this is an estimation — each factor is calculated assuming that it is the only factor to be considered, but this is not the case. The value for k would typically be around 0.5, which would dramatically increase the ZHR, giving a more accurate value for the limiting magnitude.

7.5.3 Formula improvements

Radiant height correction

An invaluable analysis would be a validation of my proposed method of calculating the radiant height correction factor. Plotting the relative meteor flux against the radiant height may reveal a better approximation to the correction factor. The issue arises in isolating variables such as the actual ZHR (which may be lower than another time of measurement) and other factors, such as changing conditions. This can largely be solved by normalizing data against the expected ZHR, or measuring these changing variables and making a comparison.

Diurnal shift correction

The diurnal shift of an observation can often be extreme, with a large range of variation over the course of 24 hours. Estimating this diurnal shift using techniques from chapter 3 will give an optimal fit sine curve, from which the expected number of meteors detected from this diurnal shift can be calculated. This will then replace the background detection count and will provide a more accurate estimate of the ZHR.

Limiting magnitude

The limiting magnitude for a radio antenna is difficult to calculate. The only practical way to work it out is to estimate based on what the antenna can be pick up. Knowing this will refine the formula further, since an accurate estimate of the limiting magnitude allows the population index to be utilised which is an important factor.

Field of view

There are techniques to estimate the field of view available to a radio antenna. If this is done, then

the formula can be improved simply by multiplying by the factor F where $F = \frac{1}{1-k}$.

7.5.4 Inaccuracies

Re-entry direction

The radio detection of a meteor largely depends on the direction it is travelling. A meteor is best detected when travelling directly across the “field of view” of the receiving antenna. It is difficult to take this into account when calculating the ZHR, but the general direction in which meteors are travelling from the radiant will have an effect on this value.

Observing station vs. transmitting antenna

There is often a marked difference between the location of the transmitting antenna and the receiving antenna, where the data is recorded. This results in a potentially large inaccuracy since the radiant altitude and other factors at the receiving station may be very different to the transmitting station.

Antenna type

When calculating the limiting magnitude and field of view, the type of antenna will influence the results greatly. Certain antennas may have a much larger field of view, or be less sensitive and have a lower limiting magnitude.

7.6 Conclusion

The ZHR formula, with modification, is valid for use in radio meteor detection. This is apparent from the good correlation between ZHR results from radio observation data when compared with visual observation, up to a constant offset. With knowledge of an antenna’s field of view, and the population index of a meteor shower, estimations can be made more accurately. Further study is required to analyse the distribution of meteor magnitudes for larger limiting magnitudes than 6.5, as well as the best way to estimate the background detection rate of an observation station. Analysis of ZHR is difficult, given the number of factors involve, and how difficult it is to isolate these factors, such as field of view.

Chapter 8

Meteor Detection by Root Mean Square Difference Image Analysis

Abstract

I discuss methods of meteor detection by image analysis focusing on root mean square difference, noting structural similarity index, edge detection, and derivatives as alternatives. I provide a quantitative measure of correlation between mean square error image analysis and established methods of radio meteor detection. I find that root mean square difference, as a comparative measure of meteor flux, correlates well with detection counts, suggesting it is a valid method of meteor detection. This provides a basic and easily adaptable alternative to existing software.

8.1 Overview

The primary method of radio meteor detection is using software to record the signal input, and compare background intensity to signal intensity across the desired frequency. Where there is a large increase in signal intensity, a meteor is considered to have been detected. An alternative to this is image analysis. This method applies a similar technique of recording the signal input, and displaying the result as a ‘waterfall’ plot (figure 8.1). Note that the frequency is not the actual frequency, since squelch is applied to the input signal. This output is saved as an image (in a format of the observer’s choosing), which can then be analysed to pick out hotspots of colour (depending on the palette used to format the image), distinct edges, or other methods. I discuss these various methods of image analysis.

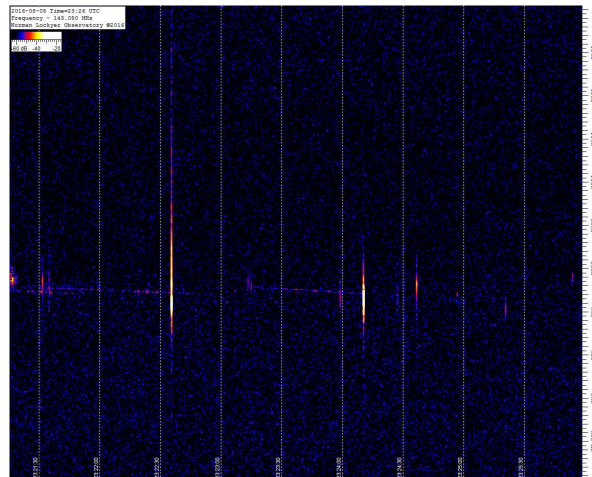


Figure 8.1: 2D waterfall plot from Spectrum Lab v3.0 [14]

8.2 Methodology

8.2.1 Root mean square difference

The general idea behind my proposed method of root mean square (RMS) difference is to compute the difference between corresponding pixels in two images: the image under consideration, and a reference image. The choice of reference image is somewhat arbitrary, as long as the same reference is used for all computations. The images that will be considered are screenshots automatically taken from SpectrumLab v3.0 [14] every minute. The meteor ‘detection’ comes from the change in the RMS difference over time. This change occurs since a meteor is represented as a yellow (or white) streak, which will significantly change the pixel values of the image. The RMS difference is the root mean square of all pixel differences. The value does not indicate exactly how many meteors have been detected, but an increase indicates a greater pixel difference, which itself indicates an increase in signal strength. An increase in signal strength is how radio meteor detection typically takes place, so the results should correlate well.

Repeated images

The input signal moves across the screen, taking 5 minutes to clear the entire window, meaning the same meteor is theoretically ‘seen’ 5 times. However, the RMS difference is a comparative measure rather than exact. The value itself has little meaning, but the change over time should indicate the change in meteor flux. This means that having the same meteor appear multiple times is beneficial, since the value may change by pure chance between each image, but repeated detections of meteors will give a distinct result in the RMS difference.

Baseline image generation

The baseline image can be generated in various ways. The aim of generating a baseline should be to minimise differences that do not contribute to the result. Namely, artefacts such as watermarks and scales which cannot be removed automatically. This can be done by averaging as many of the expected comparison images as possible. This will

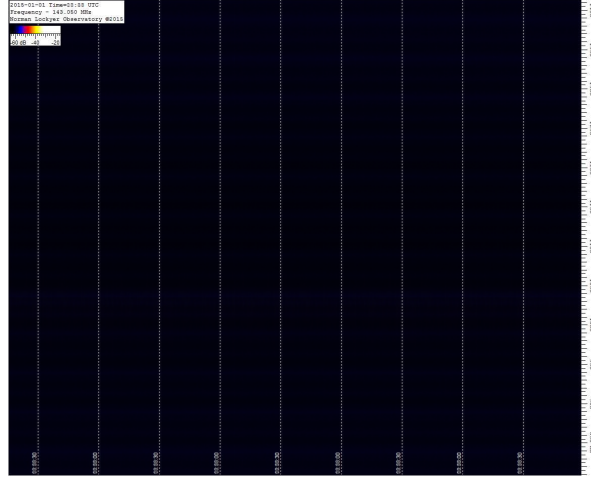


Figure 8.2: Average image for comparison baseline

result in an image similar to figure 8.2. A better baseline will be produced by including more images: I have used a sample of an entire day (1440 images) to produce figure 8.2. Alternative baseline images are as simple as a completely black image. As long as the same baseline is used, the choice is arbitrary.

RMS calculation

For my own method, the calculation is made using Python. Before the RMS difference can be calculated, a histogram of the image must be generated. This contains all possible values of the pixel values, and their associated differences between the considered image and baseline image. The root mean square of this histogram is then taken, which gives the desired result. This is repeated for each image and stored in a place of the observer’s choosing (a text file makes the most sense).

RMOB comparison

In order to test the effectiveness of this new method, I will compare the results with hourly detection counts collected using RMOB [21], for the same location, where the program running the RMS difference is implemented: the Norman Lockyer Observatory, in Devon. The RMS values are present for every minute, whereas RMOB counts are for an entire hour. In order to solve this, all the RMS differences for an hour are averaged.

8.3 Results

8.3.1 Data

The RMOB hourly detection counts are shown in figure 8.3. All available RMS values are shown in figure 8.4. There is a large gap in detection count data, which reduces the size of the data set which can be compared, however there are still 2833 pairs of values. The range of this comparison is from 2014-11-01 to 2016-11-17.

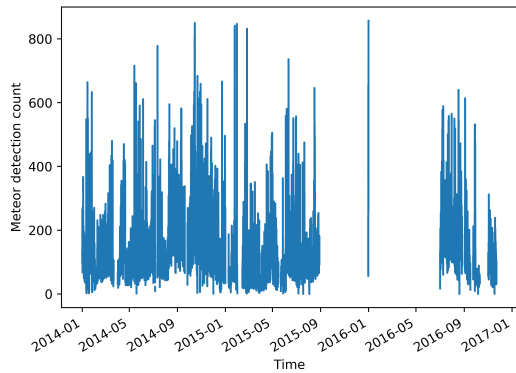


Figure 8.3: Meteor detection count (RMOB count) for NLO, Devon

It is clear from figure 8.4 that there are erroneous results for RMS differences. These can occur when the antenna is moved by wind (or by observer error) which dramatically increases the noise in the waterfall plot. This noise manifests itself as an increased blue background since there are more ‘spikes’ for frequencies outside the receiving frequency. Until the antenna is moved back to the correct position, the increased noise will persist and results in a clear offset that can be seen in figure 8.4. Other situations, such as a faulty cable or incorrect software settings, can cause similar problems.

8.3.2 Correlation

Figure 8.5 shows a scatter graph of the RMS difference against the RMOB counts. The periods with erroneous data can clearly be seen, as well as a correlation between the two sets. Even within the erroneous periods, a correlation is seen, though to

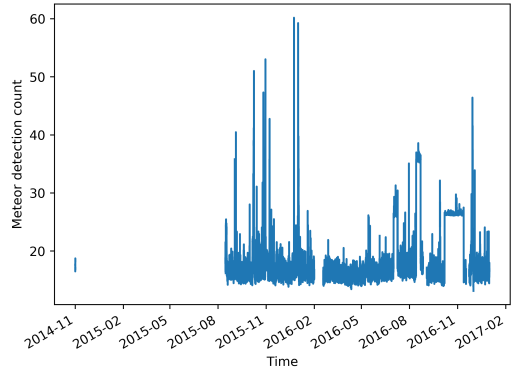


Figure 8.4: Root mean square difference against baseline for NLO, Devon

a lesser extent. This supports the idea that there is only an offset, and can likely be accounted for. However, in order to achieve a true reflection of the correlation between the two sets, I removed the erroneous data, resulting in figure 8.6. In the

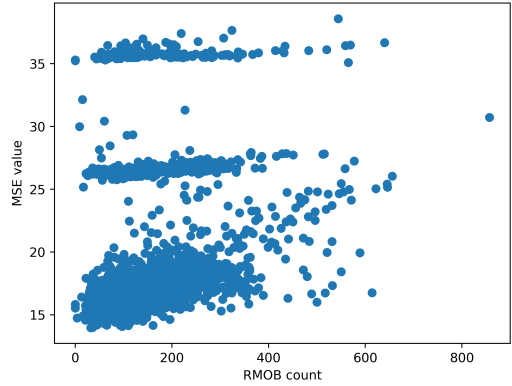


Figure 8.5: RMOB counts against RMS difference, including erroneous periods

absence of the erroneous data, the correlation becomes clearer. There are, of course, some values that do not appear to be well correlated but there is an apparent overall trend. There are 2042 pairs remaining in the data set. Using Pearson Moment Correlation Coefficient (PMCC), $r = 0.6165$, with a p-value of 4.05×10^{-214} . Therefore, with a 1% level of significance, there is evidence to suggest

there is a correlation between the two sets. The value of r indicates that there is a strong positive correlation.

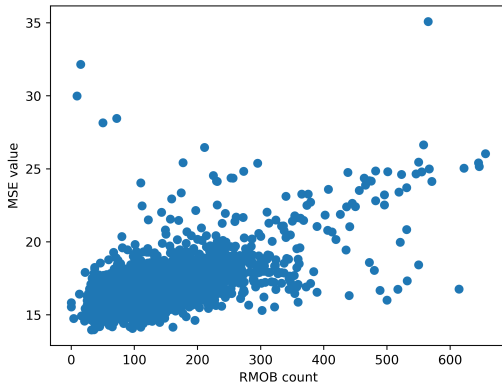


Figure 8.6: RMOB counts against RMS difference, excluding erroneous periods

8.4 Discussion

8.4.1 RMS difference

It is clear from the results that there is positive correlation, suggesting that the method is valid as a comparative measure of meteor flux. However, there are improvements that can be made to the method.

Image format

The images that are analysed in this study, are saved with a JPEG format at 50% quality. Saving as a bitmap would be much more effective, since compression would not create artefacts nor remove data that is important. This does, however, raise issues of memory space, since saving 1440 bitmap images a day will quickly fill up most storage. The best option is to process the images as bitmap, then save as JPEG.

Removing watermarks

Although an average image baseline was used to remove the influence of watermarks, simply removing them is best. This can either be done using the

software that creates the images, or an image processing technique. Removal of these watermarks & scales, variables can be further isolated, meaning the only data that should change between images is the signal being studied, improving the accuracy of results.

Frequency isolation

Theoretically, the only part of the image that should be compared is the main frequency \pm the width of the sideband (depending on whether upper or lower sideband is used). This would negate some influence of increased noise, meaning erroneous periods that occurred in the data I used are not an issue. In fact, the area of the image could be decreased further still, since the furthest edges of the sideband do not contribute much to the overall RMS difference, since the peak intensity is towards the carrier wave frequency.

Relative measure

An alternative method of negating the influence of noise is a relative measure of the RMS difference. By considering the most recent RMS differences, or by making a post-analysis pass and comparing against values before *and* after each value, the RMS difference can be normalised so that any offsets are removed.

Meteor count interpolation

Since there appears to be a correlation in the data, using a regression line would allow interpolation of meteor counts based on the RMS difference. Of course, this will have some inherent error, but as an estimation it may be useful.

8.4.2 Alternative methods

Structural similarity index measure

Structural similarity (SSIM) [9] is designed to be a better alternative to RMS difference. It is a ‘full reference’ method, meaning it requires a reference image, much like RMS difference. It measures *perceived* change in the structure of the image. This is applicable to detecting meteors from images since the changes between an image with and without a meteor are significant in terms of structure. A meteor, in a waterfall plot, is seen as a large yellow streak. This will be easily picked up by the SSIM

method since it includes a measure of variance, which will change if large pixel values are present in the image compared to a baseline. SSIM would provide a comparative measure much like RMS difference: the number of meteors in the image is not calculated, only a comparative measure of meteor flux.

Edge & blob detection

Edge detection is the process of identifying edges in an image. In combination with blob detection, the outlines of ‘blobs’ can be picked out from an image. For meteor detection this is advantageous: since meteors are represented as distinct coloured streaks, a blob with a certain shape is likely to be a meteor. This shape can be analysed using a convolution. Areas that are picked up best by the convolution, blob and edge detection can be considered as meteors. Counting the numbers of meteors will give results that can much more easily be compared to RMOB counts, indicating the effectiveness of the method.

Derivative method

Finally, I propose using derivative methods to pick out maxima in an image. This can be done by considering each row of pixels in the image, as well as each column, and calculating derivatives (most likely by forward difference), so that maxima can be identified. Picking out maxima that occur in both directions indicates a significant peak in the image. Through analysis of these results, a threshold can be picked out for the gradient required for a maximum to be considered a meteor.

8.5 Conclusion

Methods of meteor detection by image analysis, using root mean square difference, correlate well with hourly detection counts at a 1% significance level. This provides an alternative method to standard techniques of radio meteor detection, which can easily be implemented and modified to an observer’s use. I have discussed ways to improve this method to give more accurate results, providing a more valid comparative measure of meteor flux. As well as this, I have discussed alternative methods of image analysis that can provide hourly counts,

as well as methods that could provide better comparative measures than RMS difference.

Chapter 9

Conclusion

9.1 Comments

To conclude: there is yet a conclusion to be made. Throughout the 6 studies I present, small sample sizes have been an issue. Better global coverage, data over longer periods, and more data in general, would provide a much better analysis and could confirm or refute results I have found. I would like to note that this entire report is an analysis: I do not put forward explanations for all of my findings. Further modelling, analysis and investigation is a necessity. However, saying this, there are interesting findings in this report, supporting arguments for previous studies, and curious results that beg further study.

9.2 Main findings

9.2.1 Diurnal shift

- I have presented a model which fits the data. I model diurnal shift as a result of orbital velocity variations impacting incident meteor velocities.
- The peak hour of diurnal shift is at 6am local time for an observer.
- The intensity of diurnal shift appears to be uniform across the globe, with no correlation to longitude or latitude.
- There is no clear link between the amplitude of diurnal shift and latitude, though some locations have a clearly larger amplitude than others.

9.2.2 Spacial variation of data characteristics

- Data characteristics are not well correlated with latitude or longitude.
- Overall, there is little variation in data characteristics, suggesting a uniform quality of observation across the globe.
- The distribution of meteor counts is generally symmetric.

9.2.3 Temporal variation of radar counts & data characteristics

- There is a significant increase of around $2\times$ of hourly meteor detection counts between 2005 and 2011.
- The maximum in counts correlates well with a minimum in the solar cycle.
- Day-time and night-time differences in detection counts are not significant (1% significance level).
- Meteor counts increase towards the middle of the year for all observers, though this effect is most likely due to observers from the North Hemisphere, suggesting it is the summer months.
- There is little variation in meteor counts over a month.

9.2.4 Antenna data characteristics

- There is no clear correlation between data characteristics and antenna type.

- Some antennas appear to have more extreme values than others, though not significantly.
- Generally, the antenna type appears to have little impact on the quality of radio meteor detection.

9.2.5 Zenithal Hourly Rate (ZHR) validity

- Using the modifications I propose, the formula for normalising an observer's hourly rate to ZHR is valid.
- The modified formula produces radio ZHRS that correlate well with visual ZHRS.
- I present an alternative function for radiant height correction, accompanied with a geometrical argument.
- Further work is required on the validity of models of meteor shower population index.

9.2.6 Meteor detection by RMS difference image analysis

- RMS difference image analysis provides a valid comparative measure of meteor flux, which correlates well with other methods of radio meteor detection.
- RMS difference provides a suitable alternative to software that counts detected meteors.
- Alternative methods may provide an improvement, such as edge detection, or structural similarity index measures.

9.3 Acknowledgements

I am indebted to the RMOB organisation [21], from which I have sourced my data, and been given permission to complete this study. I am also grateful for the assistance of Malcolm Simpson and Ed Horncastle in the process of the studies I present.

Appendices

Appendix A

Zenithal hourly rate results

Year	Range	Mean \pm S.E.	90th %ile	Expected ZHR	Visual ZHR _{max}
2005	7/12 – 17/12	37.0 \pm 1.87	72.9	120	155
	12/12 – 16/12	43.5 \pm 3.92	85.3		
	14/12	30.6 \pm 4.03	54.4		
2006	7/12 – 17/12	44.9 \pm 2.29	83.4	120	170
	12/12 – 16/12	59.6 \pm 5.10	121		
	14/12	60.9 \pm 7.64	103		
2010	7/12 – 17/12	77.2 \pm 1.40	186	120	142
	12/12 – 16/12	97.8 \pm 2.78	237		
	14/12	124 \pm 6.53	297		
2011	4/12 – 17/12	52.2 \pm 0.995	125	120	161
	12/12 – 16/12	75.8 \pm 2.37	176		
	14/12	104 \pm 6.43	249		
2012	4/12 – 17/12	105 \pm 2.30	233	120	134
	11/12 – 15/12	144 \pm 4.55	346		
	13/12	153 \pm 7.18	355		
2013	4/12 – 17/12	56.1 \pm 1.14	134	120	133
	12/12 – 16/12	78.6 \pm 2.46	204		
	14/12	93.2 \pm 5.39	249		
2014	4/12 – 17/12	79.3 \pm 1.29	217	120	143
	12/12 – 16/12	92.1 \pm 2.52	244		
	14/12	106 \pm 4.86	270		
2015	4/12 – 17/12	56.2 \pm 1.24	132	120	163
	12/12 – 16/12	75.5 \pm 2.10	167		
	14/12	90.9 \pm 4.06	194		

Table A.1: Geminids, $r = 2.6$, RA (α) = 112° , Dec (δ) = 33°

Year	Range	Mean \pm S.E.	90th %ile	Expected ZHR	Visual ZHR _{max}
2005	14/11 – 21/11	34.7 \pm 2.36	79.0	20	24
	15/11 – 19/11	36.5 \pm 3.28	79.1		
	17/11	31.7 \pm 6.09	71.4		
2007	10/11 – 23/11	178 \pm 4.86	269	15	47
	16/11 – 20/11	194 \pm 9.25	288		
	18/11	205 \pm 17.2	288		
2010	10/11 – 23/11	58.5 \pm 1.24	151	20	21
	15/11 – 19/11	57.9 \pm 2.18	152		
	17/11	55.2 \pm 4.02	133		
2011	6/11 – 30/11	68.7 \pm 1.31	186	20	40
	16/11 – 20/11	69.5 \pm 3.31	185		
	18/11	76.9 \pm 7.94	201		
2012	6/11 – 30/11	73.8 \pm 1.85	162	15	47
	15/11 – 19/11	67.6 \pm 3.47	152		
	17/11	54.8 \pm 3.72	122		
2013	6/11 – 30/11	36.5 \pm 0.749	83.9	15	21
	15/11 – 19/11	37.5 \pm 2.09	98.5		
	17/11	42.9 \pm 4.52	114		
2014	6/11 – 30/11	53.5 \pm 0.913	150	15	19
	15/11 – 19/11	50.5 \pm 2.32	130		
	17/11	50.0 \pm 4.65	112		
2015	6/11 – 30/11	32.4 \pm 0.592	68.7	15	9
	16/11 – 20/11	30.3 \pm 1.24	62.8		
	18/11	30.1 \pm 2.38	55.9		
2016	6/11 – 30/11	31.9 \pm 0.369	74.3	15	9
	15/11 – 19/11	32.8 \pm 0.920	72.3		
	17/11	34.5 \pm 2.05	82.8		

Table A.2: Leonids, $r = 2.5$, RA (α) = 152° , Dec (δ) = 22°

Year	Range	Mean \pm S.E.	90th %ile	Expected ZHR	Visual ZHR _{max}
2010	2/10 – 7/11	63.9 \pm 0.928	162	30	56
	19/10 – 23/10	65.7 \pm 2.82	162		
	21/10	66.1 \pm 5.18	159		
2011	2/10 – 7/11	78.8 \pm 0.915	205	25	41
	19/10 – 23/10	86.4 \pm 2.87	210		
	21/10	81.5 \pm 5.63	206		
2012	2/10 – 7/11	48.5 \pm 0.626	120	25	41
	19/10 – 23/10	54.4 \pm 2.13	147		
	21/10	53.0 \pm 3.77	129		
2013	2/10 – 7/11	33.2 \pm 0.442	77.0	20	20
	19/10 – 23/10	36.2 \pm 1.38	87.8		
	21/10	37.5 \pm 2.66	85.4		
2014	2/10 – 7/11	44.3 \pm 0.571	109	18	28
	19/10 – 23/10	42.8 \pm 1.45	105		
	21/10	38.1 \pm 2.36	104		
2015	2/10 – 7/11	48.8 \pm 0.715	140	15	33
	19/10 – 23/10	54.5 \pm 2.37	156		
	21/10	53.0 \pm 4.71	150		
2016	2/10 – 7/11	33.1 \pm 0.459	83.5	15	34
	19/10 – 23/10	34.3 \pm 1.25	84.9		
	21/10	32.0 \pm 2.33	79.2		

Table A.3: Orionids, $r = 2.5$, RA (α) = 95° , Dec (δ) = 16°

Year	Range	Mean \pm S.E.	90th %ile	Expected ZHR	Visual ZHR _{max}
2010	17/7 – 24/8	71.7 \pm 1.30	183	100	142
	10/8 – 14/8	77.1 \pm 3.81	194		
	12/8	78.5 \pm 7.26	197		
2011	17/7 – 24/8	48.7 \pm 0.810	112	100	58
	11/8–15/8	53.4 \pm 2.18	116		
	13/8	68.3 \pm 4.98	141		
2012	17/7 – 24/8	61.8 \pm 1.35	114	100	122
	10/8 – 14/8	109 \pm 5.56	275		
	12/8	139 \pm 13.9	271		
2013	17/7 – 24/8	48.5 \pm 0.780	131	100	109
	10/8 – 14/8	72.6 \pm 3.20	193		
	12/8	87.2 \pm 7.09	207		
2014	17/7 – 24/8	43.3 \pm 0.575	102	100	68
	11/8–15/8	59.6 \pm 1.84	133		
	13/8	64.5 \pm 3.50	133		
2015	17/7 – 24/8	70.9 \pm 1.08	187	100	95
	11/8–15/8	74.1 \pm 3.30	180		
	13/8	91.7 \pm 7.03	193		
2016	17/7 – 24/8	36.5 \pm 0.589	91.5	100	150
	10/8 – 14/8	40.1 \pm 1.24	92.6		
	12/8	59.6 \pm 3.02	121		

Table A.4: Perseids, $r = 2.6$, RA (α) = 48° , Dec (δ) = 58°

Year	Range	Mean \pm S.E.	90th %ile	Expected ZHR	Visual ZHR _{max}
2011	1/1 – 12/1	53.7 \pm 0.550	133	120	96
	2/1 – 6/1	69.5 \pm 2.59	173		
	4/1	98.2 \pm 6.64	243		
2012	1/1 – 12/1	58.5 \pm 0.647	134	120	97
	2/1 – 6/1	58.2 \pm 2.07	136		
	4/1	104 \pm 5.64	235		
2013	1/1 – 12/1	49.2 \pm 0.488	120	120	142
	1/1–5/1	63.2 \pm 1.373	152		
	3/1	104 \pm 4.36	229		
2014	1/1 – 12/1	52.5 \pm 0.511	141	120	142
	1/1–5/1	62.5 \pm 2.70	154		
	3/1	109 \pm 7.70	282		
2015	1/1 – 12/1	39.2 \pm 0.349	97.6	120	81
	2/1 – 6/1	61.6 \pm 2.14	164		
	4/1	70.1 \pm 4.57	181		
2016	1/1 – 12/1	26.0 \pm 0.297	62.8	120	103
	2/1 – 6/1	45.6 \pm 1.31	118		
	4/1	79.9 \pm 3.27	184		

Table A.5: Quadrantids, $r = 2.1$, RA (α) = 230° , Dec (δ) = 49°

Year	Range	Mean \pm S.E.	90th %ile	Expected ZHR	Visual ZHR _{max}
2010	19/4–28/5	140 \pm 1.91	291	85	102
	4/5–8/5	149 \pm 6.77	267		
	6/5	150 \pm 14.1	304		
2011	19/4–28/5	112 \pm 1.62	260	70	95
	4/5–8/5	116 \pm 5.38	266		
	6/5	118 \pm 10.7	282		
2012	19/4–28/5	67.1 \pm 0.836	173	65	66
	3/5–7/5	72.3 \pm 2.65	199		
	5/5	72.9 \pm 5.12	197		
2013	19/4–28/5	56.1 \pm 0.889	142	55	119
	4/5–8/5	61.4 \pm 3.01	158		
	6/5	60.2 \pm 5.13	149		
2014	19/4–28/5	52.9 \pm 1.57	104	45	56
	4/5–8/5	48.5 \pm 2.87	102		
	6/5	47.4 \pm 5.03	99		
2015	19/4–28/5	50.3 \pm 0.599	114	40	64
	4/5–8/5	52.5 \pm 1.64	120		
	6/5	54.3 \pm 3.22	121		
2016	19/4–28/5	45.6 \pm 0.665	99.8	40	55
	3/5–7/5	43.3 \pm 1.51	90.3		
	5/5	46.2 \pm 3.17	95.5		

Table A.6: η -aquariids, $r = 2.4$, RA (α) = 338° , Dec (δ) = -1°

Bibliography

- [1] V. Bumba. In: *Bull. astr. Inst. Csl.* 1 (1949), p. 93.
- [2] F. L. Whipple. “A Comet Model. II. Physical Relations for Comets and Meteors”. In: *Astrophysical Journal* 113 (1951), p. 464.
- [3] Ľ. Kresák. “A Nomogram for Computing the Zenith Hourly Rates of Meteor Showers”. In: *Bull. Astron. Inst. Czechoslov.* 6 (1954), p. 120.
- [4] B. A. Lindblad. In: *Physics and Dynamics of Meteors* (1968), pp. 50–62.
- [5] V. V. Andreev, O. I. Belkovich, and V. S. Tokhtasjew. “Selection Effects in Meteor Photographic Observations”. In: *Solar System Res.* 17.4 (1983).
- [6] Brian G. Marsden. “1983 TB and the Geminid meteors”. In: *IAUC* 3881 (1983).
- [7] J. Richardson. “A Detailed Analysis of the Geometric Shower Radiant Altitude Correction Factor”. In: *WGN, Journal of the International Meteor Organization* 27.6 (1999), pp. 308–317.
- [8] W. Singer, U. von Zahn, and J. Weiß. “Diurnal and annual variations of meteor rates at the arctic circle”. In: *Atmos. Chem. Phys.* 4 (2004), pp. 1355–1363.
- [9] Z. Wang et al. “Image Quality Assessment: From Error Visibility to Structural Similarity”. In: *IEEE Transactions On Image Processing* 13.4 (2004).
- [10] W. Singer et al. “Diurnal and annual variations of meteor rates at latitudes between 69°N and 35°S”. In: *17th ESA Symposium on European Rocket and Balloon Programmes and Related Research* (2005).
- [11] Cisco. *Antenna Patterns and Their Meaning*. 2007.
- [12] NASA Cosmos and Kenneth R. Lang. *Comets produce meteor showers*. 2010. URL: https://ase.tufts.edu/cosmos/view_picture.asp?id=1305.
- [13] D. Morgan. *Meteor numbers & velocities*. 2011. URL: <http://britastro.org/radio/projects/DM-Meteor.temp/numbers.html>.
- [14] Spectrum Lab. 2016. URL: <http://www.qsl.net/dl4yhf/spectra1.html>.
- [15] Space Weather Prediction Center. *Solar Cycle Progression*. 2017. URL: <http://www.swpc.noaa.gov/products/solar-cycle-progression>.
- [16] *Detecting Meteors by Radio in Penrith, Cumbria*. URL: www.g4fui.net/meteors.html.
- [17] National Geographic, Elsevier, and M. Littmann. *1833 Meteor Storm Started Citizen Science*. URL: <http://voices.nationalgeographic.com/2014/08/30/1833-meteor-storm-started-citizen-science/>.
- [18] *HROFFT software download*. URL: <http://www.rmob.org/links.php>.
- [19] International Meteor Organization. *IMO Meteor Calendar*. Available at www.imo.net/resources/calendar/ (2017/02/15).

- [20] *Quantum Geographic Information System*. URL: www.qgis.org.
- [21] *Radio Meteor Observation Bulletin*. URL: rmob.org.
- [22] Sky Scan. *Radio wave propagation*. URL: www.skyscan.ca/HowItWorks.htm.